Leishmania Dual Specificity Tyrosine Regulated Kinase 1 (DYRK1) is required for sustaining Leishmania stationary phase phenotype

Running Title: LinDYRK1 is essential for Leishmania stationary phase biology

Vinícius Pinto Costa Rocha[1,2], Mariko Dacher[3#a], Simon Alan Young[4], Foteini Kolokousi[5], Antonia Efstathiou[5], Gerald Frank Späth[3], Milena Botelho Pereira Soares[1,2]*, Despina Smirlis[5]*

[1]Instituto Gonçalo Moniz, Fundação Oswaldo Cruz (FIOCRUZ), Rua Waldemar Falcão 121, Salvador, BA, Brazil;

[2]Centro de Biotecnologia e Terapia Celular, Hospital São Rafael, Avenida São Rafael 2152, Salvador, BA, Brazil;

[3]Unité de Parasitologie Moléculaire et Signalisation, Department of Parasites and Insect Vectors, Institut Pasteur and INSERM U1201, Paris, France;

[4]Biomedical Sciences Research Complex, School of Biology, The University of St. Andrews, North Haugh, St. Andrews, Fife, Scotland, UK;

[5]Molecular Parasitology Laboratory, Microbiology Department, Hellenic Pasteur Institute, 127 Bas. Sofias Avenue, Athens, Greece;

[#a]Current address: Laboratory of Chromatin Structure and Function, Institute for Quantitative Biosciences, The University of Tokyo, Yayoi 1-1-1, Bunkyo-ku, Tokyo, Japan.

This article has been accepted for publication and undergone full peer review but has not been through the copyediting, typesetting, pagination and proofreading process, which may lead to differences between this version and the Version of Record. Please cite this article as doi: 10.1111/MMI.14464

Address correspondence to: **1**: Despina Smirlis, Department of Microbiology, Laboratory of Molecular Parasitology, Hellenic Pasteur Institute, 127 Bas. Sofias Avenue, 115 21 Athens, Greece, Tel.: +30 2106478841 Fax: +30 2106423498; e-mail address: penny@pasteur.gr; **2**: Milena Botelho Pereira Soares, Instituto Gonçalo Moniz, Fundação Oswaldo Cruz (FIOCRUZ), Rua Waldemar Falcão 121, Salvador, BA, Brazil; [2]Centro de Biotecnologia e Terapia Celular, Hospital São Rafael, Avenida São Rafael 2152, Salvador, BA, Brazil, Tel: Phone: (+55)71-31762292, email: milena@bahia.fiocruz.br, milenabpsoares@gmail.com

Keywords: Leishmania, DYRK1, kinase, growth, stationary

Summary

Although the multiplicative and growth-arrested states play key roles in Leishmania development, the regulators of these transitions are largely unknown. In an attempt to gain a better understanding of these processes, we characterised one member of a family of protein kinases with dual specificity, LinDYRK1, which acts as a stasis regulator in other organisms. LinDYRK1 over-expressing parasites displayed a decrease in proliferation and in cell cycle re-entry of arrested cells. Parasites lacking LinDYRK1 displayed distinct fitness phenotypes in logarithmic and stationary growth phases. In logarithmic growth-phase, LinDYRK1$^{-/-}$ parasites proliferated better than control lines, supporting a role of this kinase in stasis, while in stationary growth-phase, LinDYRK1$^{-/-}$ parasites had important defects as they rounded up, accumulated vacuoles and lipid bodies and displayed subtle but consistent differences in lipid composition. Moreover, they expressed less metacyclic-enriched transcripts, displayed increased sensitivity to complement lysis and a significant reduction in survival within peritoneal macrophages. The distinct LinDYRK1$^{-/-}$ growth phase phenotypes were mirrored by the distinct LinDYRK1 localisations in logarithmic (mainly in flagellar pocket area and endosomes) and late stationary phase (mitochondrion). Overall, this work provides first evidence for the role of a DYRK family member in sustaining promastigote stationary phase phenotype and infectivity.

Keywords: Leishmania**,** DYRK, differentiation, cell cycle, growth arrest

Introduction

Leishmania is a protozoan parasite responsible for a group of diseases, termed leishmaniases, that shows multiple clinical manifestations, ranging from self-healing cutaneous to lethal visceral leishmaniasis if left untreated (Murray et al., 2005). These diseases are endemic in tropical and

subtropical countries, causing severe morbidity and mortality and presenting a worldwide incidence of approximately 1 500 000 clinically reported cases (Alvar et al., 2012).

Leishmania spp have a digenetic life cycle, involving a motile, extracellular promastigote stage that parasitises the alimentary tract of a sand-fly vector, and an immotile amastigote stage that survives and replicates in the phagolysosomes of mononuclear phagocytes (Bates, 1994, Sacks & Perkins, 1984). To complete its life cycle, the parasite has to successfully undergo different developmental transitions induced by environmental stimuli. In the midgut of the sand-fly, sequential development of promastigotes inside the sugar-rich environment initially involves the rapid division of non-infective procyclic promastigotes (Burchmore & Barrett, 2001, McConville & Naderer, 2011). These parasites differentiate into distinct forms, including the cell cycle arrested nectomonads and the dividing leptomonads that will ultimately differentiate to infective, metacyclic promastigotes in the anterior parts of the digestive tract (Gossage et al., 2003). During a blood meal, metacyclics will be transmitted to the mammalian host, where they will encounter a marked environmental temperature (26˚C to 34-37˚C) and pH (7.4 to 5.5) shift, as well as changes in nutrients including a sugar-poor and fatty-acid- and amino-acid-rich environment. Parasites that will successfully adapt to these new environmental changes and subvert the immune system of the host will differentiate and proliferate as amastigotes (Burchmore & Barrett, 2001, McConville & Naderer, 2011).

Leishmania promastigote differentiation in the sand-fly requires homeostatic control and signalling events that are largely unknown (Sacks & Perkins, 1984, Sacks & Perkins, 1985). Procyclic to metacyclic promastigote transitions in the sand fly can be mirrored in cell culture (Gossage et al., 2003) and are characterised by specific molecular, morphological, biochemical and cell cycle changes (Inbar et al., 2017, Sacks et al., 1985, Sacks & Perkins, 1984, Sacks & Perkins, 1985). These transitions are initiated by environmental changes (Cunningham et al., 2001, Serafim et al., 2012), and are communicated by signalling cascades, including phosphosignalling events (Tsigankov et al., 2014, Tsigankov et al., 2013). Despite the importance

of phosphosignalling in differentiation, there is little knowledge on the nature of kinases that mediate these transitions. Amongst these, protein kinase A (PKA) activity is known to be required for the promastigote to amastigote transition (Bachmaier et al., 2016), whereas Target of Rapamycin (TOR) 3 is known to be associated with the development of the infectious stage (Madeira da Silva & Beverley, 2010).

The dual specificity tyrosine regulated kinases (DYRKs) are members of the CMGC group of kinases (Kannan & Neuwald, 2004) are characterised by their dual specificity, presenting an auto-phosphorylation activity of a critical tyrosine residue of the activation loop and a serine/threonine kinase activity towards substrates (Becker & Joost, 1999). Based on the homology of their kinase domain, these proteins are divided into 3 subfamilies: the homeodomain-interacting protein kinases (HIPKs) known to regulate a wide variety of stress signals (Schmitz et al., 2014), the pre-mRNA processing protein 4 kinases (PRP4s) involved in pre-mRNA processing and transcriptional regulation (Huang et al., 2000) and the DYRKs (Aranda et al., 2011). The DYRK subfamily comprises of the YAKs, class I (DYRK1A and DYRK1B) and class II (DYRK2, DYRK3 and DYRK4) DYRKs (Aranda et al., 2011).

The DYRK subfamily members are multifaceted kinases, regulating a great variety of cellular processes including gene expression, proteasomal degradation, or chromatin remodelling (Aranda et al., 2011). Stasis regulation and differentiation however, is the hallmark of DYRK activity (Aranda et al., 2011). The DYRK subfamily shares a conserved structure which includes a DYRK homology (DH) box, an aspartic rich sequence that precedes the kinase domain (Becker & Joost, 1999), a characteristic HCD motif in the catalytic loop, instead of the highly conserved HRD (Kannan & Neuwald, 2004), and a YxY motif with the second tyrosine being auto-phosphorylated and required for DYRK activity (Lochhead et al., 2005). Regulatory sequences including nuclear localisation sequences (NLSs) and a PEST sequence known to act as signal for protein degradation., are present in specific members of the DYRK family (Aranda et al., 2011).

Recently, a role in differentiation was shown for a DYRK related kinase of the trypanosomatid parasite Trypanosoma brucei. Mony et al performed a genome-wide RNAi target screen to identify genes whose down-regulation resulted in a cAMP unresponsive phenotype (Mony et al., 2014). This phenotype was associated with a differentiation defect, whereby parasites failed to differentiate from the "proliferative slender" to the "arrested stumpy" form, the latter stage being responsible for transmission to the tsetse flies (Mony et al., 2014). In addition, another DYRK member from T. brucei has been shown to be required for parasite survival in the mouse (Fernandez-Cortes et al., 2017).

Interestingly, in Leishmania the DYRK family consists of 8 members. DYRK1 homologue (LinJ.15.0180, LinDYRK1) is a single-copy gene which has the highest conservation to mammalian DYRK1A and DYRK1B orthologues. Herein, we combined genetic manipulation and phenotypic analyses to generate null mutants and report that LinDYRK1 is a pro-survival kinase and its deletion is associated with a deregulated stationary phase biology.

Results

Evolutionary relationship and characterisation of Leishmania DYRK family members

To investigate the identity and evolutionary relationship of Leishmania DYRK family proteins, we employed phylogenetic analyses of animal, plant, insect, yeast and protist DYRK protein sequences. Our analysis revealed the presence of 8 Leishmania DYRK proteins, in accordance to previous reports (Parsons et al., 2005). From the Leishmania DYRK members, five belong to all three DYRK subfamily groups, namely the DYRK (LinJ.15.0180-LinDYRK1, LinJ.14.0890 and LinJ.33.1930), the HIPK (LinJ.19.0360) and the Prp4 (Lin.J.36.4460) **(Fig 1A**). The other three family members (LinJ.21.2010, LinJ.14.1140 and LinJ.35.1850) did not cluster with the known DYRK subfamilies (**Fig 1A**).

LinDYRK1 possesses sequences, including the HCD triplet in the catalytic loop and a Tyrosine (HRY^{523}), aligning to the second tyrosine of the DYRK subfamily activation loop sequence YxY, which conform to DYRK constraints (**Fig 1B**, **S1 Fig**). In addition, LinDYRK1 is more similar to mammalian DYRKs than to lower eukaryotic YAKs. For example, LinDYRK1 is closer in sequence identity to H. sapiens (Hs) DYRK1A (48.5% identity, query cover 97%, E value: $1*e^{-63}$) and HsDYRK1B (49.5%, query cover: 96%, E value: $4*e^{-65}$), than to S. cerevisiae Yak1p (46.55% identity, query cover 59%, E value: $1*e^{-35}$).

In Leishmania, the kinase with the highest similarity to LinDYRK1 is LinJ.14.0890 (**Fig 1B**). The full protein sequences share an overall 54% sequence identity (54% query cover, E value: 8e-74), while both proteins have a long N terminal domain of unknown function, unique to Leishmania. The two kinases lack a NLS and contain predicted PEST sequences (**Fig 1B**). The DH box, while conserved in LinDYRK1, is not present in LinJ.14.0890, whereas LinJ.14.0890 also possesses a conserved tyrosine (PKY^{743}), in its predicted activation loop. This kinase however, has insertions in the activation loop between subdomains VII and VIII and between subdomains X and XI (**Fig 1B**), and thus its catalytic activity merits experimental validation.

Apart from LinJ.14.0890, other Leishmania DYRK family members have important modifications of consensus sequences within the kinase domain. For example, LinJ.21.2010 and LinJ.14.1140 are characterised by the atypical glycine rich loops DXAXXSXXV and GXAXXSXXV respectively, that replace the highly conserved GXGXXGXV required for the positioning of ATP (**S2 Fig**). Interestingly, LinJ.19.0360 contains an atypical DFS cation binding site instead of the highly conserved DF/LG (**S2 Fig**) and thus the catalytic activities of these kinases require confirmation.

LinDYRK1 localisation

To investigate the subcellular localisation of LinDYRK1, we expressed a tagged version of LinDYRK1 with eGFP at its N-terminus (GFP-LinDYRK1) from an episome. In logarithmic

cultures, LinDYRK1-GFP was mainly localised at the anterior side of the cell. Co-localisation with mitotracker was used in an attempt to compare LinDYRK1 localisation in logarithmic cells with respect to the mitochondrion. Our results showed that GFP-LinDYRK1 in logarithmic cells, exhibited no co-localisation with mitotracker (**Fig 2A**). Moreover, concanavalin A (ConA) conjugated to Alexa594 (ConA–Alexa594) used to label the surface glycocalyx and the flagellar pocket (Ilgoutz et al., 1999), revealed that GFP-LinDYRK1 occupied a portion of the flagellar pocket area (**Fig 2B**). GFP-LinDYRK1 was also found outside the flagellar pocket at the anterior end of the kinetoplast (**Fig 2B**) and between the nucleus and kinetoplast (**Fig 2A** and **Fig 2B**). In order to further investigate the localisation of LinDYRK1 in logarithmic cells, FM4-64 dye was used as a marker of endosomes (Besteiro et al., 2006). Areas of intense localisation of GFP-LinDYRK1 were observed, similar to the localisation of FM4-64, in a 3 min pulse chase experiment followed by an incubation time of 20 min incubation at RT **(Fig 2C)**. GFP-LinDYRK1 in late logarithmic/ early stationary phase promastigotes extended more throughout the cell body (**Fig 2A**) but showed a distinct localisation with respect to mitotracker (**Fig 2A**). In late (stationary phase day 7 of cell culture, day 3 of stationary phase) however, we observed a change in GFP-LinDYRK1 localisation to areas, where mitotracker was present (**Fig 2A**).

To ensure that the observed LinDYRK1 localisation was not an artefact, we expressed from an episome a second fusion protein, tagged with eGFP at its C-terminus (LinDYRK1-GFP). LinDYRK1-GFP had a similar localisation to GFP- LinDYRK1 (**S3A** and **S3B Fig**). Despite the fact that episomal expression can sometimes cause excessive expression of the target protein, that might result in potential mislocalisation (Tanz et al., 2013), this does not seem to be the case in our system. The levels of N and C terminal tagged fusion proteins were much lower than GFP, and below the detection limit by western blot analysis in total protein extracts (data not shown). In addition, the fact that similar localisation for both C and N terminal fusion proteins was observed, is a strong indication that they represent the localisation of the endogenous protein.

LinDYRK1 over-expression has a negative effect on promastigote growth

To have a better understanding of the LinDYRK1 function, we created a L. infantum cell line that over-expresses the protein from a Leishmania expression plasmid (pXNG4). This plasmid expresses Herpes Virus Thymidine kinase (HSV-TK) and can be subject to negative selection by antiviral drug gancinclovir (GCV), which is phosphorylated by HSV-TK into a toxic product (Murta et al., 2009). Parasites over-expressing LinDYRK1 {LinDYRK1$^{+/+}$[pXNG-LinDYRK1]} had a proliferation defect with respect to control parasites {wild type (LinDYRK1$^{+/+}$), parasites that had lost the episome after treatment with GCV {LinDYRK1$^{+/+}$[pXNG-LinDYRK1]} and parasites transfected with plasmid alone {LinDYRK1+/+[pXNG]} visible at seeding density of 10^6 mL^{-1} **(Fig 3A)**. In order to measure more precisely the growth defect, a lower seeding density was used (3 *10^5 mL^{-1}) for LinDYRK1$^{+/+}$[pXNG-LinDYRK1] and LinDYRK1$^{+/+}$[pXNG] promastigotes. The logarithmic slopes of the growth curves were compared and our results demonstrated that LinDYRK1 over-expressing parasites proliferated 33% less well than parasites bearing plasmid alone **(Fig 3A)**. Cell cycle progression of LinDYRK1 over-expressing parasites was also investigated by initially synchronising LinDYRK1$^{+/+}$[pXNG-LinDYRK1] and LinDYRK1$^{+/+}$[pXNG] promastigotes at the G_0/G_1-S boundary with an inhibitor of ribonucleotide reductase, hydroxyurea (HU). Subsequently cell cycle re-entry was allowed by removal of HU. Cell cycle was investigated 0 h, 3 h and 6.5 h after HU removal. At 6.5 h post HU removal 51% of LinDYRK1$^{+/+}$[pXNG-LinDYRK1] parasites had not entered in S-G2/M phases in contrast to only 15% of control LinDYRK1$^{+/+}$[pXNG] parasites (**Fig 3B, S1 Table**), and revealed that LinDYRK1 over-expression resulted in delayed cell cycle re-entry of resting cells.

LinDYRK1 gene deletion is tolerated in logarithmic phase promastigotes

Assuming initially that LinDYRK1 was essential, we decided to generate LinDYRK1 facilitated knockouts, a process that overcomes a potentially lethal phenotype (Dacher et al., 2014, Murta et

al., 2009). The episome [pXNG4] mentioned above, also expresses GFP, which is used as a reporter for monitoring its loss (Dacher et al., 2014, Murta et al., 2009). By sequentially introducing the puromycin N-acetyl-transferase (PAC) and then the hygromycin B (HYG) targeting cassettes, we replaced the two LinDYRK1 alleles in L. infantum promastigotes transfected with [pXNG-LinDYRK1] (**S4A Fig**). Following this strategy, we generated two homozygous facilitated mutants from two independent heterozygous clones (**A** and **B**). We confirmed incorporation of the targeting of cassettes into the LinDYRK1 genomic locus by diagnostic PCR (**S4B Fig**).

We then tested if LinDYRK1 was essential for promastigote survival. To this end, we applied negative selection by replacing the positive selection drug NTC with the negative selection drug GCV and analysed the loss of the episome by measuring the GFP fluorescence by flow cytometry. Analysis of the GFP fluorescence of both clones **A** and **B** for 4 passages in logarithmic phase revealed that the LinDYRK1 expressing episome could be eliminated after the addition of GCV, in a similar manner to the episome in wild type promastigotes (**Fig. 4A**). Moreover, the mean GFP fluorescence was reduced gradually to levels similar to wild type LinDYRK1$^{+/+}$ promastigotes (**Fig 4B**). To be certain that the loss of fluorescence in the pools of parasites correlated with the loss of the [pXNG-LinDYRK1] episome, we analysed by western blotting the GFP amounts of individual clones isolated after 15 passages of cell-culture, using alpha-tubulin as a loading control (**Fig 4C**). We did not observe GFP expression in any of the clones tested (**Fig 4C**), revealing that LinDYRK1$^{-/-}$ parasites can be viable without the episome, while GFP was detected in the control LinDYRK1$^{+/+}$[pXNG-LinDYRK1] pool treated with NTC (**Fig 4C**). To rule out the possibility of an extra copy of LinDYRK1 anywhere within the genome of L. infantum, we performed diagnostic PCR with internal LinDYRK1 primers (p1 and p2) in selected clones after GCV selection, and failed to amplify a product (**S4C Fig**). Overall, our findings showed that the loss of the [pXNG-LinDYRK1] episome could be tolerated in logarithmic cells and that LinDYRK1 is not essential for viability.

The experiment was also repeated without the presence of the episome, in order to ascertain that GCV does not alter the phenotype of these cells. We were able to generate and LinDYRK1$^{-/-}$ promastigotes, termed direct heterozygous LinDYRK1$^{+/-direct}$ and direct homozygous LinDYRK1$^{-/-direct}$ mutants. Correct incorporation of targeting cassettes and lack of internal LinDYRK1 copy were validated by PCR (**S4D Fig**).

LinDYRK1 deletion affects stationary growth phase

To further investigate the biological role of LinDYRK1, we analysed the phenotype of LinDYRK1$^{-/-}$ parasites, including growth comparisons. In the logarithmic phase clones LinDYRK1$^{-/-}$**B1** and LinDYRK1$^{-/-}$**B2** displayed a higher proliferation rate (40% and 66% for clones **B1** and **B2** respectively) and higher maximal cell density than their parental cell line LinDYRK1$^{-/-}$[pXNG-LinDYRK1]**B** (**S5A Fig**). A higher proliferation was also observed for LinDYRK1$^{-/-}$**A1** and LinDYRK1$^{-/-}$**A2** clones with respect to their parental line (data not shown). In addition, growth comparison between a LinDYRK1**A1**$^{-/-}$ add back cell line and LinDYRK1**A1**$^{-/-}$ promastigotes transfected with plasmid alone {LinDYRK1$^{-/-}$[pXNG]}, revealed that add backs displayed 30% reduced proliferation rate and lower maximal cell density (**S5B Fig**). Moreover, the homozygous LinDYRK1$^{-/-direct}$ also proliferated better than the heterozygous LinDYRK1$^{+/-direct}$ **(S5C Fig**). These results altogether, allow us to conclude that the lack of LinDYRK1 has a positive effect on the growth rate of logarithmic cells.

Despite the fitness of LinDYRK1$^{-/-}$ mutants in logarithmic growth phase, in stationary phase these cells displayed defects including morphological alterations. All experiments in stationary growth phase, were performed the second day of stationary growth phase, unless stated otherwise. Stationary LinDYRK1$^{-/-}$ parasites, were less elongated, had greater width and were more rounded than wild type, parental LinDYRK1$^{-/-}$[pXNG-LinDYRK1] lines and an add back clone (**Fig 5A**). Similar morphological alterations were observed with direct null mutants (**S6A Fig**). Flow cytometry analysis confirmed these findings which showed higher forward scatter

(FSC) values for both facilitated LinDYRK1$^{-/-}$ **(S6B Fig)** and the LinDYRK1$^{-/-direct}$ mutants **(S6C Fig)** in comparison to control promastigotes. Moreover, null mutants in stationary phase accumulated a greater percentage of cells with two nuclei (N) and two kinetoplasts (K) (17% and 29% of clones LinDYRK1$^{-/-}$**A1** and LinDYRK1$^{-/-}$**A2**, respectively), and a greater percentage of cells with 2N1K (7% and 12.5% for clones LinDYRK1$^{-/-}$**A1** and LinDYRK1$^{-/-}$**A2**, respectively) versus ≤3.3% of 2N2K and ≤1% of 2N1K of control cells (parental line LinDYRK1$^{-/-}$[pXNG-LinDYRK1]**A** and LinDYRK1$^{+/+}$) (**S6D Fig**). This could be an indication that these promastigotes are in a stress related G_2/M cell cycle arrest, which in due time results in cell death (Azzopardi et al., 2017).

Cell death was increased in late stationary phase in facilitated and direct LinDYRK1$^{-/-}$ clones (**Fig 5B**, **S7 Fig, Table S2A**). For facilitated clones LinDYRK1$^{-/-}$**A1** and LinDYRK1$^{-/-}$**A2**, 46.3% and 33.8% respectively had hypodiploid DNA content, versus 4.9% of wild type LinDYRK1$^{+/+}$, 15.2% of LinDYRK1$^{-/-}$ [pXNG-LinDYRK1]**A** and 9% of LinDYRK1$^{-/-}$**A1**[pXNG-LinDYRK1] add back (**Fig 5B, Table S2A**). In early stationary phase (day 5 of growth curve, day 1 of stationary phase) LinDYRK1$^{-/-}$ mutants did not show increase of hypodiploid DNA content (**S7A Fig),** whereas late stationary phase (day 7 of growth curve, day 3 of stationary phase).

LinDYRK1$^{-/-}$ stationary phase promastigotes exhibit severe surface aberrations, lipid body formation and display notable lipid content changes

To further investigate the morphological defects of LinDYRK1$^{-/-}$ parasites in stationary phase, we performed scanning (SEM) and transmission (TEM) electron microscopy. SEM analysis of facilitated LinDYRK1$^{-/-}$ mutants revealed had surface aberrations, with folds on the surface and membrane invaginations (**Fig 6A**). TEM analysis revealed that LinDYRK1$^{-/-}$ promastigotes displayed an abnormal subcellular structure. These parasites exhibited intense vacuolisation of the cytoplasm, (**Fig 6B**{III, IV, V, VI}). Vacuoles often contained membrane blebs, where the kinetoplast membrane dissociated inside a vacuole (**Fig 6B**{V}). Another

prominent ultrastructural feature of LinDYRK1$^{-/-}$ parasites was the presence of lipid vacuoles or bodies observed by their low electron density and homogeneous appearance (Charron & Sibley, 2002). Lipid bodies were found to be adjacent to vacuoles and often were merging with the cell membrane, leaving an open invagination full of lipids (**Fig 6B** {III and IV}). In addition some parasites had fragmented DNA **(Fig 6B** IV), suggesting that they were already in the process of cell death.

As lipid droplet formation may be linked to lipid metabolism (Walther & Farese, 2012), we further investigated the lipid composition of LinDYRK1$^{-/-}$ promastigotes. To this end, we analysed the total phospholipid content by nano-electrospray mass spectrometry (nESI-MS), and by gas chromatography mass spectrometry (GC-MS) the total fatty acid and sterol content. We analysed two knockout clones LinDYRK1$^{-/-}$**A** and LinDYRK1$^{-/-}$**B** from different parental strains to normalise for colony specific effects, and compared them with wild type parasites (LinDYRK1$^{+/+}$) and the parental clone LinDYRK1$^{-/-}$[pXNG-LinDYRK1] **A**. Our results showed that LinDYRK1 mutants had higher amounts of saturated fatty acids (**Fig. 6C**, **Table 1**). The most evident difference was a decrease in the percentage of 18:2, and an increase in that of 18:0 (**Table 1**), resulting in a C18:2/C18:0 fatty acid ratio of ~0.7 and ~0.8 for the clones LinDYRK1$^{-/-}$**A1** and LinDYRK1$^{-/-}$**B1** respectively, versus 1.7 for wild type cells. Furthermore, sterol analysis showed that LinDYRK1$^{-/-}$parasites displayed relatively lower cholesterol levels than the pool of LinDYRK1$^{+/+}$ parasites (14-15% mutants versus 27% wild type) and higher ergosta-7,24-dien-3β-ol levels (17.8%-22% mutants versus 11% wild type) (**Table 1**). Finally, our analysis demonstrated that LinDYRK1 knockout does not significantly affect phospholipid composition (**S8 Fig**).

LinDYRK1$^{-/-}$ promastigotes exhibit defects in markers of infective promastigotes, increased thermosensitivity and reduced survival in host macrophages

To ensure survival within the mammalian host, Leishmania promastigotes develop resistance to complement-mediated lysis, as they progress from the logarithmic to stationary growth phase (Franke et al., 1985). In an attempt to relate LinDYRK1$^{-/-}$ stationary phase defects with parasite infectivity, the ability of null mutants to endure complement lysis in logarithmic and stationary phase was assessed. LinDYRK1$^{-/-}$ promastigotes were more susceptible to complement lysis (70% logarithmic and 30% stationary phase) than LinDYRK1$^{+/+}$ (46.7% logarithmic and 17.8% stationary phase) and LinDYRK1$^{-/-}$[pXNG-LinDYRK1] (53% logarithmic and 16.5 % stationary phase) promastigotes (**Fig 7A**).

The number of infective metacyclics and the expression of metacyclic enriched transcripts were also measured for stationary phase LinDYRK1$^{-/-}$ mutants and control cells. For measuring metacyclics, the peanut agglutinin (PNA) assay was performed, which relies on the ability of the PNA lectin to bind and agglutinate non-infective procyclics but not infective metacyclic promastigotes (Sacks et al., 1985). The assay revealed that that the percentage of unagglutinated LinDYRK1$^{-/-}$ parasites was 2.8 times less than wild type LinDYRK1^{+}/$^{+}$ and 3.6 times less than LinDYRK1$^{-/-}$[pXNG-LinDYRK1] (**Fig 7B**). In addition, LinDYRK1$^{-/-}$ parasites expressed less well transcripts known to be enriched in metacyclic promastigotes. More specifically levels of prohibitin {LinJ.16.1710 (Almeida et al., 2004)}, meta1 {LinJ.17.0990, (Nourbakhsh et al., 1996)} and HASPB {LinJ23.1220} (Sadlova et al., 2010)} transcripts normalised with ribosomal protein S29 transcript (LinJ.28.2360) were compared. The ratios of normalised transcripts were significantly reduced with respect to wild type LinDYRK1$^{-/-}$ **A1** (7.14 fold less for prohibitin, 5 fold less for meta1 and 4.17 fold less for HASPB) and to LinDYRK1$^{-/-}$ [pXNG-LinDYRK1]**A** (2.57 fold less for prohibitin, 2.6 fold less for meta1and 1.46 less for HASPB) (**Fig. 7C**). These results suggest that stationary phase defects are not only morphological in LinDYRK1$^{-/-}$ but also biochemical, and are consistent with defects in metacyclogenesis.

In addition to metacyclogenesis, other factors may influence stage differentiation as the ability to survive a 26→37^{o}C upshift in temperature, which mimics the sand-fly to mammalian

host temperature transition. As DYRK related kinases are known to regulate thermotolerance (Hartley et al., 1994), we hypothesised that LinDYRK1$^{-/-}$ promastigotes were less thermotolerant. We subjected parasites to a 16 h 26→37^{o}C heat-shock and compared the percentage of hypodiploid cells in facilitated (**Fig 7D**, **S2C Table**) and direct mutants (**S2D Table, S6 Fig**) with the corresponding control cells. Our analyses showed that all LinDYRK1 knockouts were more sensitive to heat-shock than control cell lines **(Fig 7D**, **S7 Fig, S2C&D Table**). More specifically 28% and 29% of LinDYRK1$^{-/-}$ clones **A1** and **A2** had hypodiploid DNA content, versus 17.1% of the parental strain, 16.12% of the LinDYRK1$^{-/-}$[pXNG-LinDYRK1] add back and 12.5% of the wild type LinDYRK1$^{+/+}$ promastigotes **(Fig 7D**, **S2C&D Table**). Comparison of direct mutants also confirmed that lack of LinDYRK1 gave rise to a more thermosensitive phenotype **(S9 Fig**, **S2C&D Table**), reinforcing that heat shock sensitivity is specifically related to loss of LinDYRK1 expression.

We then performed an in vitro infection assay and compared the percentage of infection and survival of LinDYRK1$^{-/-}$, LinDYRK1$^{-/-}$[pXNG-LinDYRK1] and LinDYRK1$^{+/+}$ stationary phase parasites in murine peritoneal macrophages. The infection rate of LinDYRK1$^{-/-}$ parasites (% of infected macrophages and number of parasites per macrophage) was dramatically reduced by 10.5-fold (2.7 less % infected macrophages and 3.9 times less parasites per macrophage) 72 h post infection, compared the beginning of infection (**Fig 7E**). The controls, LinDYRK1$^{+/+}$ and LinDYRK1$^{-/-}$[pXNG-LinDYRK1], presented similar rates or moderate reduction of infection rates 72 h post infection compared to the beginning of infection (**Fig 7E**). In addition, we attempted to measure the in vivo infectivity of these parasites. To this end, efforts were made to recover freshly isolated wild type and transgenic parasites cultivated in parallel, from livers of BALB/c mice. During these attempts, it was possible to recover only LinDYRK1$^{-/-}$ [pXNG-LinDYRK1] parasites in one of the three mice used per group. Parasite burden of animals infected was measured two weeks post-infection by qPCR using liver DNA to estimate the amount of the Leishmania specific arginine permease gene AAP3 (Tellevik et al., 2014) and corresponded to

1530 parasites per 8700 hepatocyte nuclei. This result is suggestive of the reduced ability of LinDYRK1$^{-/-}$ promastigotes to survive in mice, as the ability of parasites to survive in mice is compromised even in wild type background parasites due to the continuous cultivations and manipulations.

Discussion

In this work, we determined the evolutionary relationship of the Leishmania DYRK family members. A clustering of Leishmania DYRK family members both within (for 5 out of 8), and outside (for 3 out of 8) of the known subfamilies (DYRKs, HIPKs, Prp4s), suggests that the DYRK taxonomy in its current form, requires revisiting and the inclusion of a more representative repertoire of eukaryotic organisms. Differences in highly conserved sequences (glycine rich loop, cation binding site) of the kinase catalytic domain for specific Leishmania DYRK family members indicate that these are either pseudokinases or kinases with atypical features mirroring the unique biology of the parasite. LinDYRK1 is one of the genes that shares all the features of an active kinase, and recombinant LinDYRK1 has been shown to be an active kinase (Hombach-Barrigah et al., 2019).

LinDYRK1 had a distinct localisation in logarithmic, stationary and late stationary growth phases. LinDYRK1 localisation in proliferative and early stationary phases, in the flagellar pocket area, a structure known to carry out endo- and exo-cytosis (Stierhof et al., 1994) and endosomes involved in endocytic cycle (Besteiro et al., 2006) and mitochondrial localisation in late stationary phase, show that LinDYRK1 signaling is growth stage dependent. The endosomal localisation data is reminiscent of a known role for mammalian DYRK1A in endocytosis and vesicle recycling (Murakami et al., 2009, Murakami et al., 2012).

In this study, it was shown that LinDYRK1 knockouts were viable and that in the logarithmic growth phase had a higher proliferation rate than control cell lines. At the same time,

over-expression of LinDYRK1 in Leishmania resulted in decreased proliferation and delayed cell cycle re-entry after synchronisation by HU. These results could be in line with the known role of DYRKs in various cell types, in regulating the decision between cell cycle re-entry and cell cycle exit (Soppa & Becker, 2015) in mitogen-poor environments (Becker, 2018, Garrett & Broach, 1989). In Leishmania however, further enquiry is needed to address if there is a direct role for LinDYRK1 in cell cycle control and proliferation, including the identification of partners and substrates.

One of the most prominent phenotypes observed in this study was the deregulated phenotype of stationary phase LinDYRK1$^{-/-}$ mutants. Stationary phase phenotypes in unicellular organisms are known to have activated the internal systems of protection against stress and are able to survive better under adverse or changing environmental settings (Pletnev et al., 2015). In Leishmania too, stationary phase promastigotes have increased ability to survive in the intracellular environment of the mammalian host (Wozencraft & Blackwell, 1987) and this ability is associated with metacyclogenesis (da Silva & Sacks, 1987). In our system LinDYRK1$^{-/-}$ stationary phase promastigotes displayed several defects. Knockout parasites were more round and exhibited an intense vacuolisation of the cytoplasm. The formation of vacuoles in wild type cells could be the result of an ongoing autophagic process, a survival process (Smirlis et al., 2010) that also occurs during the procyclic to metacyclic promastigote stage differentiation (Williams et al., 2006). Prolonged, autophagy results in cell death (Smirlis et al., 2010), and could explain the cell death observed in long range stationary phase promastigotes.

The accumulation of lipid bodies and the switch in the ratio of saturated (18:0) and polyunsaturated (18:2) fatty acids in stationary phase LinDYRK1$^{-/-}$ promastigotes, may be related to the formation of lipid bodies, as this switch of identical lipids in mammalian cells corroborates to the formation of large lipid droplets (Arisawa et al., 2016). Most importantly, large lipid droplets are induced by stress (Petan et al., 2018), while changes in relative ratios of saturated fatty acids are anticipated in normal procyclic to metacyclic stage differentiation (Silva et al.,

2011). Hence our results suggest abnormal differentiation processes and/or stress response. Sterol metabolism is also known to be affected differentially in Leishmania logarithmic and stationary phase cultures (Jacobs et al., 1982). The decrease observed for the relative amount of cholesterol in LinDYRK1$^{-/-}$ parasites, is suggestive of a disruption in uptake. This is less explainable for the parent cell line LinDYRK1$^{-/-}$[pXNG-LinDYRK1] but even in these cells some vacuolisation is visible. Conversely, the alteration in sterol composition may be entirely due to upregulation of the synthesis of some of endogenous ergostane-based sterols, clearly visible in the putative terminal molecule of the pathway, ergosta-7,24-dien-3β-ol (Yao & Wilson, 2016).

In addition, defects in metacyclogenesis, infectivity and thermotolerance of LinDYRK1$^{-/-}$ parasites mirror the importance of the kinase in the completion of the Leishmania life-cycle. The enrichment of the S. cerevisiae YAK1 in differentiated quiescent yeast stationary-phase cultures (Aragon et al., 2008) and its thermoprotective function in yeast (Hartley et al., 1994), may reveal a central role of DYRK kinases in stationary phase biology and thermoprotection.

Overall, our findings suggest that LinDYRK1 signalling is needed to normal promastigote development. This finding is one step further for gaining insight into the contribution of protein phosphorylation in the growth-stress response balance. It opens new areas of research and future challenges, including the identification of DYRK1 substrates and investigation of the role of LinDYRK1 in the amastigote stage.

Experimental Procedures

Multiple sequence alignment

To search DYRK kinases in Leishmania, BLAST analysis was performed with blastp algorithm using protein sequences of known DYRK genes from H. sapiens, D. melanogaster, S. cerevisiae as queries. Sequences from L. infantum, T. cruzi and T. brucei were retrieved from the NCBI (http://www.ncbi.nlm.nih.gov/protein/) and TriTrypDB databases (http://tritrypdb.org/tritrypdb/).

Protein alignment was performed using CLUSTALW 2.0.12 using the built-in programs (Bioedit). Unrooted phylogenetic tree defined by amino acid sequence similarities was generated using Interactive Tree of Life (http://itol.embl.de/). Sequence accession numbers are shown in **S3 Table**.

Plasmids

For the generation of [pXNG-LinDYRK1] construct, the open reading frame (ORF) of LinDYRK1 (LinJ.15.0180) was amplified by polymerase chain reaction (PCR) from L. infantum (L4, MHOM/GR/78/L4) genomic DNA and cloned into the Leishmania expression plasmid [pXNG4]. To this end, the p1/p2 primer pair (**S4 Table**) were used and LinDYRK1 ORF was cloned into the BglII (New England Biolabs) site of [pXNG4] plasmid.

LinDYRK1 targeting constructs, encoding for HYG and PAC resistance markers to antibiotics hygromycin B and puromycin respectively, flanked by the ~ 900 bp 5' and 3' UTR of the LinDYRK1 gene, were generated for replacing the genomic LinDYRK1 ORF. To this end, the 900 bp 5'-UTR and 3'-UTR of LinDYRK1were PCR-amplified using primer pairs p3/p4 and p5/p6, respectively (**S4 Table**), and cloned by TA cloning in the appropriate orientation into [pGEM-T] and [pGEM-T Easy] vectors (Promega) respectively, resulting in pGEM-5'UTR and [pGEM-T Easy-$^{3'}$UTR] plasmids. The LinDYRK1 3'UTR was released using NotI restriction enzyme (New England Biolabs) and cloned into the NotI site of pGEM-5'UTR in the appropriate orientation, to generate plasmid [pGEM-5'UTR-3'UTR]. HYG and PAC coding sequences were PCR-amplified from plasmids [pX63-Hyg] and [pXG-PAC], using primer pairs p7/p8 and p9/p10 and cloned into the SpeI/BamHI restriction sites of [pGEM-5'UTR-3'UTR]. Primers p3 and p6 also contained an internal PmeI (**S4 Table**) restriction site, which was used for the generation of linear constructs prior to electroporation.

To generate a GFP-LinDYRK1 fusion construct, the LinDYRK1 insert was sub-cloned from [pXNG-LinDYRK1] in the BglII site of [pXG-GFP^{+2}] plasmid. To generate the [LinDYRK1-GFP] fusion construct, the LinDYRK1 insert encoding the ORF was amplified by PCR from genomic L. infantum (L4, MHOM/GR/78/L4) DNA with the use of the p1/p21 primer pair (**S4 Table**). The PCR product was digested with BglII and BamHI and inserted in the appropriate orientation in the BamHI site of [PXG-PAC] Leishmania expression plasmid to generate plasmid [LinDYRK1-carboxyterminal]. The eGFP was PCR amplified from [pEGFP(N3)] (Clontech®) using the p22/ p23 primers pair (**S4 Table**), digested with BamHI and BglII. The product was cloned in the appropriate orientation in the BamHI site of plasmid [LinDYRK1-carboxyterminal], to generate plasmid [pXG-PAC-LinDYRK1-GFP]. All constructs were confirmed by sequencing.

Cell culture and transfection

L. infantum L4 strain (L4, MHOM/GR/78/L4) promastigotes were cultivated at 26° C in M199 medium supplemented with 10% foetal bovine serum, 100 µM adenine, 10 µg mL^{-1} hemin, 40 mM HEPES (N-2-hydroxyethylpiperazine-N'-2-ethanesulfonic and acid) (pH 7.4), and 50 units of Penicillin-Streptomycin (Gibco Laboratories) (Kapler et al., 1990) and L. amazonensis parasites (MHOM/BR88/BA-125, Leila strain) were cultured in cultured in Schneider's insect medium (Sigma Aldrich, St. Louis, MO) supplemented with 10% fetal bovine serum (Gibco Laboratories, Gaithersburg, MD).

Parasite transfection was performed in logarithmic phase promastigotes that were washed in electroporation buffer (21 mM HEPES pH 7.5, 137 mM NaCl, 5 mM KCl, 0.7 mM Na_2HP0_4 and 6 mM glucose) and transfected by electroporation with 20 µg of plasmids DNA ([pXNG-LinDYRK1] , pXG-GFP-LinDYRK1] or [pXG-PAC-LinDYRK1-GFP]), according to previously established protocols (Beverley & Clayton, 1993). Parasites transfected with [pXNG-LinDYRK1]

and [pXGGFP^{+2}-LinDYRK1] constructs were selected in fully supplemented culture medium in the presence of 150 μg mL^{-1} NTC, 50 μg mL^{-1} G418 and 30 μg mL^{-1} puromycin, respectively.

For the generation of LinDYRK1 facilitated mutants, we followed the methodology described (Dacher et al., 2014). More specifically, LinDYRK1$^{+/+}$[pXNG-LinDYRK1] L. infantum promastigotes were first transfected with 3 μg of PmeI linearised and dephosphorylated PAC targeting cassette. Parasites were plated 12 h post transfection in solid medium (fully supplemented M199 containing 1% (w/v) noble agar, 60 μg mL^{-1} puromycin and 100 μg mL^{-1} NTC. Two independent clones were selected to check for correct PAC cassette genomic integration. Integration was validated by PCR using genomic DNA of the two colonies as template and primers p14/p11 (**S4 Table**). After the confirmation of the cassette replacement into the DYRK1 genomic locus, two independent LinDYRK1$^{+/-}$[pXNG-LinDYRK1] heterozygous clones **A** and **B**, were transfected with 3μg of PmeI linearised and dephosphorylated HYG targeting cassette and selected in solid medium (see above), which contained 60 μg mL^{-1} puromycin, 60 μg mL^{-1} hygromycin B and 100 μg mL^{-1} NTC. Representative homozygous clones derived from both **A** and **B** heterozygous clones were selected and analysed for the correct integration of the HYG replacement cassette and the absence of genomic LinDYRK1 ORF with the primer pairs p14/p12 and p14/p13, respectively (**S4 Table**). For generating "direct knockouts", the same procedure was performed in wild type cells that had not been previously transfected with the construct [pXNG-LinDYRK1].

To negatively select against [pXNG-LinDYRK1], the NTC antibiotic was replaced by 50 μg mL^{-1} of GCV in LinDYRK1$^{-/-}$[pXNG-LinDYRK1] and LinDYRK1$^{+/+}$[pXNG-LinDYRK1] parasites, used as control, as previously described (Dacher et al., 2014). For passive loss of the [pXNG-LinDYRK1] episome, the NTC antibiotic was omitted from the culture medium. For selecting single colonies parasites were plated on M199 agar plates (Dacher et al., 2014).

Promastigote growth was assessed microscopically by counting fixed cells daily in a malassez cell-counting chamber or by flow cytometry. All growth curve experiments were performed at least three times.

SDS-polyacrylamide gel electrophoresis (SDS-PAGE) and immunoblotting

SDS-polyacrylamide gel electrophoresis (SDS-PAGE) was performed by the method of Laemmli (Laemmli, 1970). For immunoblotting, proteins were transferred on a nitrocellulose filter (Hybond C, Amersham Biosciences) and immunoblotting was performed as previously described (Papageorgiou & Soteriadou, 2002). For the analysis of GFP expression, we performed immunoblotting using monoclonal mouse antibodies anti-GFP (Miltenyi) and mouse anti-α tubulin (Sigma), both at 1:2000 dilution. A mouse horseradish peroxidase-conjugated antibody (Pierce) was finally added, and the image acquired by ECL® Plus (enhanced chemiluminescence) (GE Healthcare), according to the manufacturer's instructions. After the development of the first signal corresponding to GFP, the blots were stripped and reprobed with anti-tubulin antibody.

Flow cytometry

For measuring the GFP fluorescence of live parasites, parasites were incubated with 50 μg mL^{-1} propidium iodide (PI). GFP was analysed in the FL1 channel or 525/40 BP filter and PI in FL2 or 610/20 BP of FACS Calibur (Becton Dickinson) and Cytoflex 5 (Beckman Coulter), respectively. For cell cycle analysis, logarithmic parasites were synchronised in the G_1/S boundary with 2.5 mM of HU (Sigma Aldrich) for 12 h, as previously reported. The DNA content of promastigotes was analysed by PI staining of RNAse A treated and ethanol fixed parasites, as previously described (Smirlis et al., 2006, Hombach-Barrigah et al., 2019). More specifically, cells were fixed by addition of ice-cold ethanol and parasitic DNA content was measured by flow cytometry following the incubation with 50 μg mL^{-1} PI and 100 μg mL^{-1} RNase A (Invitrogen) in PBS in

554 the FL2 or 610/20BP channels. For all experiments 10,000 events were collected and analysed.
555 Flow Jo (Miltenyi), MODFIT (Becton-Dickinson) and CELLQuest™ (Becton-Dickinson)
556 software were used to perform the analyses. All flow cytometry experiments were performed at
557 least three times and results presented are from one representative experiment.
558
559 **Fluorescence microscopy**
560 For immunofluorescence analysis, L. infantum promastigotes were incubated with 4% (w/v)
561 paraformaldehyde (PF) for 30 min at room temperature (RT). Cells were left to adhere in poly L-
562 lysine coated slides for 20 min. Parasites were blocked with 1% (w/v) BSA in PBS (Sigma
563 Aldrich) and permeabilised with 0.1% (v/v) triton X-100 (Sigma Aldrich) for 30 min and
564 subsequently stained with 1:200 diluted in PBS/ 0,1% (w/v) BSA, mouse anti-alpha tubulin
565 antibody (Sigma, 051M4771) followed by 1 μg mL^{-1} anti-mouse IgG antibody conjugated with
566 Alexa Fluor® 594. Prior to mounting parasites were stained with 2 μM Hoechst 33342 for 15
567 min. Slides were mounted in Vectashield (Vector Laboratories).
568 Analysis of the localisation of LinDYRK1 fusions with eGFP, was performed with
569 staining of live cells with ConA-Alexa594 (Molecular Probes), MitoTracker® Orange
570 CMTMRos (Thermo Fisher Scientific) and FM®4-64FX (Molecular Probes), aided with DNA
571 co-staining with 16 μM Hoechst 33342 (Molecular Probes) according to the manufacturer's
572 instructions. In brief, promastigotes were incubated with 5 μg mL^{-1} of ConA and 20 μg mL^{-1}
573 FM4-64 for 3 min on ice followed by incubation at RT at various time points , and with 100 nM
574 mitotracker for 30 min at RT. ConA stained promastigotes were subjected to live imaging while
575 MitoTracker Orange and FM4-64 stained cells were fixed with 4% (w/v) PF and mounted, as
576 previously reported.
577 Images were collected using the ApoTome inverted (ZEISS) and the confocal
578 microscopes FluoView 1000 (Olympus; Tokyo, Japan) and TCS SP8P (Leica Microsystems

GmbH, Germany). For analysing the morphology of the parasites, images were collected and analysed in Image J software.

Transmission and scanning electron microscopy

Parasites in stationary growth phase were fixed in a solution of 2.5% (v/v) glutaraldehyde, 2 % (v/v) formaldehyde and 2.5 mM $CaCl_2$ in 0.1 M sodium cacodylate buffer pH 7.2, followed by post-fixation in 1% osmium tetroxide and 0.8 % potassium ferrocyanide in the same buffer and acetone gradient dehydration. Finally, the material was embedded in Poly/Bed resin; ultrathin sections were stained with uranyl acetate and lead citrate and observed under a JEM 1320 transmission electron microscope (JEOL). For scanning electron microscopy, parasites were fixed as abovementioned and washed in 0.1 M cacodylate buffer. Cells were left to adhere in poly L-lysine coated slides for 20 min, and post-fixed with a solution of osmium tetroxide containing 0.8–1% of potassium ferrocyanide for 30 min and dehydrated with increasing concentrations of ethanol (30%, 50%, 70%, 90% and 100% (v/v). Samples were subjected to the critical point, metalised with gold and analysed in a JEOL JSM-6390LV scanning electron microscope.

Lectin-mediated agglutination and complement lysis

Agglutination assays using PNA (100 μg μL^{-1}; Sigma) were performed as previously described (Sacks et al., 1985). Stationary phase (day 2 stationary phase) were washed 2 times in PBS and incubated at a density of $3*10^8$ mL^{-1} with PNA in PBS at RT for 30 min and the suspension was centrifuged at 150 x g for 5 min.

Complement lysis of promastigotes was performed according Späth et al., 2003 (Späth et al., 2003). Promastigotes (10^6), were washed and incubated for 30 minutes in 10% (v/v) human serum, that previously separated by centrifugation at 6,000 x g from clotted donor blood, and 50

μg mL^{-1} propidium iodide (Sigma). The percentage of fluorescence (lysis) was determined by flow cytometry.

cDNA synthesis and real-time quantitative reverse transcription-PCR

First strand cDNA was synthesised from 1 μg total RNA using the (Protoscript M-MuLV Taq RT-PCR kit, New England Biolabs) with oligo(dT)18 primers following the manufacturer's instructions. The resulting cDNA was diluted 5 times (10 ng mL^{-1}) with nuclease-free water (NEB). 50 ng of cDNA template were used in a final volume of 20 μL 1X SYBR Green (Kappa Biosystems) based quantitative PCR reactions on a SaCycler-96 RUO cycler (Sacace Biotechnologies, Italy). The protocol used for the qPCR was: 10 s at 94°C, 40 cycles comprising of 30 s at 94°C, 20 s at 52°C, 30 s at 72°C, and a final step of 10 min at 4°C. Primer pairs p15-p16, p17-p18 and p19-p20 were used to amplify meta 1 transcript (LinJ.17.0990), HASPB (LinJ.23.1220) and prohibitin (LinJ.16.1710) respectively (**S4 Table**). The sequences of primer pairs for ribosomal protein S29 transcript (LinJ.28.2360) have been previously described (Alexandratos et al., 2013). Gene expression levels were calculated using the comparative C_t method as previously described (Alexandratos et al., 2013), from duplicate or triplicate PCRs of cDNAs synthesised from RNAs recovered from parasites in three different experiments.

Infection of mice and determination of parasite burden with quantitative real-time polymerase chain reaction (qPCR)

Male BALB/c mice (6–8 weeks old) used in the present study were obtained from the breeding unit of the Hellenic Pasteur Institute (HPI; Athens, Greece) and reared in institutional facilities under specific pathogen-free environmental conditions at an ambient temperature of 25°C. Mice were provided with sterile food and water ad libitum. Stationary-phase promastigotes were harvested by centrifugation at 800× g for 10 min at 4°C. The pellet was washed by PBS and

resuspended at a concentration of 4×10^8 cells mL-1. A volume of 100 µL of this preparation was injected intravenously in the lateral tail vein of each mouse. Two weeks post infection, mice were sacrificed by CO_2 asphyxiation and 2 mg of liver tissues were frozen for subsequent analysis. DNA was extracted from about 2 mg of liver tissue from infected mice using NucleoSpin® DNA Rapid Lyse (Macherey-Nagel) according to the manufacturer's instructions. Parasite burden was determined using TaqMan-based qPCR assay as previously described (Margaroni et al., 2017, Tellevik et al., 2014). Briefly, the assay was performed in the presence of 15 pmol of forward (5′-7GGCGGCGGTATTATCTCGAT-3′) and 5 pmol of reverse (5′-ACCACGAGGTAGATGACAGACA-3′) primers (VBC Biotech, Vienna, Austria) (targeting a 74- bp region of the gene encoding the arginine transporter AAP3 gene) and 25 pmol of TET-labeled TaqMan® probe (TET-5′-ATGTCGGGCATCATC-3′-BHQ; VBC Biotech) and DNA template (50 ng and 100 ng) in a TaqMan master mix (2×) (Kapa Biosystems, Wilmington, MA, USA). Each qPCR test was run in triplicate on a SaCycler-96 RUO cycler (Sacace Biotechnologies, Como, Italy). The cycling conditions were 95°C for 10 min, followed by 40 cycles at 95°C, 15 s and 62°C, 60 s. The standard curve method for absolute quantification of parasite number was used. Quantification was performed using standard curves prepared from DNA extracted from ten-fold serial dilution of L. infantum parasites (range $1–1\times10^5$).

Macrophage infection

Peritoneal macrophages exudate from 6- to 8-week-old female BALB/c mice were collected after 4 days injection of 3% (v/v) thioglycollate (Sigma Aldrich), as described previously (Gomes et al., 2003). Macrophages were obtained by flushing the peritoneal cavity once with 10 mL ice-cold saline and centrifuged at 300 × g for 10 min. Cells were resuspended in complete RPMI medium, seeded at $2*10^5$/well in 24 well plates containing 13mm-rounded glass slides, and incubated at 37°C, 5% CO_2 overnight. Stationary phase L. infantum parasites were plated at a parasite:host cell ratio of 10:1 and incubated for 24 h (time zero) at 37° C 5% CO_2. Infected

cultures were washed extensively with PBS and incubated at the same conditions during 24, 48 and 72 h. Cultures were then fixed with 4% (w/v) paraformaldehyde. DNA was marked with 3 μM DAPI (Sigma Aldrich). Plates were incubated at RT for 10 min followed by wash with PBS. In vitro macrophage infections were performed in triplicates in at least three independent experiments. One hundred macrophages were counted per replicate.

Lipid extraction and analysis

Total lipids were extracted from L. infantum by the Bligh and Dyer method (Bligh & Dyer, 1959). Briefly, cells in stationary phase were collected by centrifugation (800×g, 10 min), washed with PBS, resuspended in 100 μL PBS and transferred to a glass tube. Following the addition of 375 μL of 1:2 (v/v) $CHCl_3$: MeOH the samples were vortexed thoroughly before further vigorous agitation for 1 hour at 4°C. Biphasic mixtures were generated by the addition of 125 μL of $CHCl_3$ with vortexing and then 125 μL of H_2O again with vortexing followed by centrifugation at 1000×g at RT for 5 min. The lower chloroform-rich phase was transferred to a new glass vial, dried under nitrogen and stored at 4°C. The lipid extracts were dissolved in 50 μL choloroform:methanol (1:2), 50 μL of acetonitrile:isopropanol:water (6:7:2) and 10 mM ammonium acetate and analysed with a Sciex 4000 QTrap, a triple quadrupole mass spectrometer equipped with an AdvionTriVersaNanoMate® source. The nanoelectrospray interface allowed the delivery of samples by direct infusion (~125 nL min^{-1}) with lipids analysed in both positive and negative ion modes using a capillary voltage of 1.25 kV with each spectrum encompassing at least 50 repetitive scans. Tandem mass spectra (MS/MS) were obtained for precursors of phosphatidylinositol (PI)/inositol-phosphoceramide (IPC) species in negative ion mode, with parent-ion scanning of m/z 241 (collision energy of 70V); and phosphatidylcholine (PC)/ sphingomyelin (SM) species in positive mode, with parent-ion scanning of m/z 184 (collision energy of 50V). Assignment of phospholipid species is based upon a combination of survey, daughter and precursor scans, as well as previous assignments (Fernandez-Prada et al., 2016,

Richmond et al., 2010) and use of the LIPID MAPS: Nature Lipidomics Gateway (www.lipidmaps.org).

Identification and characterisation of fatty acids

Total fatty acids were isolated from the L. infantum lipid extracts and converted to fatty acid methyl esters (FAME) for GC-MS characterisation following the method of Ichihara and Fukubayashi (2010) (Ichihara & Fukubayashi, 2010). This trans-methylation reaction forms methyl esters of all fatty acids in the sample, regardless of the lipid they were attached to. Briefly, lipid samples were resuspended in 300 µL of 8% (w/v) solution of HCl in methanol water (85:15 v/v) and 200 µL of toluene and 1.5 mL of methanol were added prior to incubation overnight at 45°C. Samples were dried down under nitrogen and 500 µl hexane and 500 µl distilled water were added to create a biphasic mixture, of which the FAME containing upper hexane layer is extracted and dried again under nitrogen. FAME samples were dissolved in 20 µL dichloromethane and analysed by injection of 1 µL into a Agilent Technologies GC-MS (GC-6890N, MS detector-5973) using a ZB-5 column (30 Mx 25 mm x 25mm, Phenomenex) with a temperature program of 50°C for 10 min followed by a rising gradient to 220°C at 5°C /min and hold at 220°C for a further 15 min. Mass spectra were continuously acquired in the range of 50-500 amu and peak identification was performed by comparison of the retention times and fragmentation patterns with a bacterial FAME standard mixture that contains a cyclopropyl C19Δ FAME, in addition to common fatty acids (SIGMA Supelco 47080-U).

Identification and characterisation of sterols

L. infantum lipid extracts were resuspended in 100 µL dichloromethane with 1 µL analysed by gas chromatography-mass spectrometry (GC-MS) on an Agilent Technologies mass selective detector (GC-6890N, MS detector-5973) with a ZB-50 column (15 M x 32 mm ID x 0.5 mm

thickness, (Phenomenex), injector at 270°C with a temperature program of 100°C for 1 min followed by a rising gradient to 200°C at 8°C /min and hold at 200°C for a further 2 min, followed by a second gradient at 3°C /min up to 300°C for a further 15 min. Electron ionisation (EI) was at 70 eV energy, with an emission current of 50 μA and an ion source of 230°C. Mass spectra were acquired from 50-550 amu. Identification was carried out by comparison of the retention times and fragmentation patterns with sterols in the NIST/EPA/NIH Mass Spectral Library and those reported in previous publications (Cauchetier et al., 2002, Fernandez-Prada et al., 2016, Yao & Wilson, 2016). To examine changes in composition, the area under each sterol peak was used for relative quantification.

Ethics statement

All animal protocols were conducted in strict accordance with the National Law 56/2013, which adheres to the European Directive 2010/63/EU for animal experiments, and complied with the Animal Research: Reporting of In Vivo Experiments (ARRIVE) guidelines. The study was carried out according to the approved by the Ministry of Rural Development and Food license no. 433-01-2018. The human blood donor sampled was an author of this project. The Bioethics Committee of Hellenic Pasteur Institute was aware of experiments that required human blood in this project, and a waiver was received prior to the initiation of experiments (no.3156).

Acknowledgments

The authors would like to thank Prof. Stephen Beverley for the [pXNG4], [pXGGFP+2], [pXG-PAC] and [pX63-HYG] plasmids and Laura Piel for designing and donating primers p15-p20. The authors would like to thank the Flow Cytometry and Microscopy Units of Hellenic Pasteur Institute and Dr Evangelia Xingi for the help provided, in microscopy analysis. This work was supported by the International Division of the Institute Pasteur (ACIP A13-2013 project), the

Action “KRIPIS I” (MIS 450598) co-financed by European Union and the National Ministry of Education and Religion Affairs under the Operational Strategic Reference Framework (NSRF 2007-2013) and the General Secretariat of Research and Technology (GSRT) and FAPESB/CAPES grant # PET0042/2013 from the Brazilian State and Federal governments, respectively.

Conflict of Interest

None of the authors of the above manuscript has declared any conflict of interest.

Author contributions

VPCR, MD, SAY, GFS, MBPS and DS have made major contributions to the conception or design of the study, VPCR,MD, SAY, FK, AE, GFS, MBP and DS to the acquisition, analysis, or interpretation of the data; VPCR GFS, SAY, MBPS and DS to the writing of the manuscript.

Data Availability Statement

The data that supports the findings of this study are available in the supplementary material of this article.

References

Alexandratos, A., J. Clos, M. Samiotaki, A. Efstathiou, G. Panayotou, K. Soteriadou & D. Smirlis, (2013) The loss of virulence of histone H1 overexpressing Leishmania donovani parasites is directly associated with a reduction of HSP83 rate of translation. Mol Microbiol **88**: 1015-1031.

Almeida, R., B.J. Gilmartin, S.H. McCann, A. Norrish, A.C. Ivens, D. Lawson, M.P. Levick, D.F. Smith, S.D. Dyall, D. Vetrie, T.C. Freeman, R.M. Coulson, I. Sampaio, H. Schneider & J.M. Blackwell, (2004) Expression profiling of the Leishmania life cycle: cDNA arrays identify developmentally regulated genes present but not annotated in the genome. Mol Biochem Parasitol **136**: 87-100.

Alvar, J., I.D. Velez, C. Bern, M. Herrero, P. Desjeux, J. Cano, J. Jannin, M. den Boer & W.H.O.L.C. Team, (2012) Leishmaniasis worldwide and global estimates of its incidence. PLoS One **7**: e35671.

Aragon, A.D., A.L. Rodriguez, O. Meirelles, S. Roy, G.S. Davidson, P.H. Tapia, C. Allen, R. Joe, D. Benn & M. Werner-Washburne, (2008) Characterization of differentiated quiescent and nonquiescent cells in yeast stationary-phase cultures. Mol Biol Cell **19**: 1271-1280.

Aranda, S., A. Laguna & S. de la Luna, (2011) DYRK family of protein kinases: evolutionary relationships, biochemical properties, and functional roles. FASEB J **25**: 449-462.

Arisawa, K., H. Mitsudome, K. Yoshida, S. Sugimoto, T. Ishikawa, Y. Fujiwara & I. Ichi, (2016) Saturated fatty acid in the phospholipid monolayer contributes to the formation of large lipid droplets. Biochem Biophys Res Commun **480**: 641-647.

Azzopardi, M., G. Farrugia & R. Balzan, (2017) Cell-cycle involvement in autophagy and apoptosis in yeast. Mechanisms of ageing and development **161**: 211-224.

Bachmaier, S., R. Witztum, P. Tsigankov, R. Koren, M. Boshart & D. Zilberstein, (2016) Protein kinase A signaling during bidirectional axenic differentiation in Leishmania. Int J Parasitol **46**: 75-82.

Bates, P.A., (1994) The developmental biology of Leishmania promastigotes. Exp Parasitol **79**: 215-218.

Becker, W., (2018) A wake-up call to quiescent cancer cells - potential use of DYRK1B inhibitors in cancer therapy. The FEBS journal **285**: 1203-1211.

778 Becker, W. & H.G. Joost, (1999) Structural and functional characteristics of Dyrk, a novel
779 subfamily of protein kinases with dual specificity. Prog Nucleic Acid Res Mol Biol **62**: 1-
780 17.
781 Besteiro, S., R.A. Williams, L.S. Morrison, G.H. Coombs & J.C. Mottram, (2006) Endosome
782 sorting and autophagy are essential for differentiation and virulence of Leishmania major.
783 J Biol Chem **281**: 11384-11396.
784 Beverley, S.M. & C.E. Clayton, (1993) Transfection of Leishmania and Trypanosoma brucei by
785 electroporation. Methods Mol Biol **21**: 333-348.
786 Bligh, E.G. & W.J. Dyer, (1959) A rapid method of total lipid extraction and purification. Can J
787 Biochem Physiol **37**: 911-917.
788 Burchmore, R.J. & M.P. Barrett, (2001) Life in vacuoles--nutrient acquisition by Leishmania
789 amastigotes. Int J Parasitol **31**: 1311-1320.
790 Cauchetier, E., P.M. Loiseau, J. Lehman, D. Rivollet, J. Fleury, A. Astier, M. Deniau & M. Paul,
791 (2002) Characterisation of atovaquone resistance in Leishmania infantum promastigotes.
792 Int J Parasitol **32**: 1043-1051.
793 Charron, A.J. & L.D. Sibley, (2002) Host cells: mobilizable lipid resources for the intracellular
794 parasite Toxoplasma gondii. J Cell Sci **115**: 3049-3059.
795 Cunningham, M.L., R.G. Titus, S.J. Turco & S.M. Beverley, (2001) Regulation of differentiation
796 to the infective stage of the protozoan parasite Leishmania major by tetrahydrobiopterin.
797 Science **292**: 285-287.
798 da Silva, R. & D.L. Sacks, (1987) Metacyclogenesis is a major determinant of Leishmania
799 promastigote virulence and attenuation. Infect Immun **55**: 2802-2806.
800 Dacher, M., M.A. Morales, P. Pescher, O. Leclercq, N. Rachidi, E. Prina, M. Cayla, A.
801 Descoteaux & G.F. Späth, (2014) Probing druggability and biological function of
802 essential proteins in Leishmania combining facilitated null mutant and plasmid shuffle
803 analyses. Mol Microbiol **93**: 146-166.

Fernandez-Cortes, F., T.D. Serafim, J.M. Wilkes, N.G. Jones, R. Ritchie, R. McCulloch & J.C. Mottram, (2017) RNAi screening identifies Trypanosoma brucei stress response protein kinases required for survival in the mouse. Sci Rep **7**: 6156.

Fernandez-Prada, C., I.M. Vincent, M.C. Brotherton, M. Roberts, G. Roy, L. Rivas, P. Leprohon, T.K. Smith & M. Ouellette, (2016) Different Mutations in a P-type ATPase Transporter in Leishmania Parasites are Associated with Cross-resistance to Two Leading Drugs by Distinct Mechanisms. PLoS Negl Trop Dis **10**: e0005171.

Franke, E.D., P.B. McGreevy, S.P. Katz & D.L. Sacks, (1985) Growth cycle-dependent generation of complement-resistant Leishmania promastigotes. J Immunol **134**: 2713-2718.

Garrett, S. & J. Broach, (1989) Loss of Ras activity in Saccharomyces cerevisiae is suppressed by disruptions of a new kinase gene, YAKI, whose product may act downstream of the cAMP-dependent protein kinase. Genes Dev **3**: 1336-1348.

Gomes, I.N., A.F. Calabrich, S. Tavares Rda, J. Wietzerbin, L.A. de Freitas & P.S. Veras, (2003) Differential properties of CBA/J mononuclear phagocytes recovered from an inflammatory site and probed with two different species of Leishmania. Microbes Infect **5**: 251-260.

Gossage, S.M., M.E. Rogers & P.A. Bates, (2003) Two separate growth phases during the development of Leishmania in sand flies: implications for understanding the life cycle. Int J Parasitol **33**: 1027-1034.

Hanks, S.K. & T. Hunter, (1995) Protein kinases 6. The eukaryotic protein kinase superfamily: kinase (catalytic) domain structure and classification. FASEB J **9**: 576-596.

Hartley, A.D., M.P. Ward & S. Garrett, (1994) The Yak1 protein kinase of Saccharomyces cerevisiae moderates thermotolerance and inhibits growth by an Sch9 protein kinase-independent mechanism. Genetics **136**: 465-474.

Hombach-Barrigah, A., K. Bartsch, D. Smirlis, H. Rosenqvist, A. MacDonald, F. Dingli, D. Loew, G.F. Späth, N. Rachidi, M. Wiese & J. Clos, (2019) Leishmania donovani 90 kD Heat Shock Protein - Impact of Phosphosites on Parasite Fitness, Infectivity and Casein Kinase Affinity. Sci Rep **9**: 5074.

Huang, Y., T. Deng & B.W. Winston, (2000) Characterization of hPRP4 kinase activation: potential role in signaling. Biochem Biophys Res Commun **271**: 456-463.

Ichihara, K. & Y. Fukubayashi, (2010) Preparation of fatty acid methyl esters for gas-liquid chromatography. J Lipid Res **51**: 635-640.

Ilgoutz, S.C., K.A. Mullin, B.R. Southwell & M.J. McConville, (1999) Glycosylphosphatidylinositol biosynthetic enzymes are localized to a stable tubular subcompartment of the endoplasmic reticulum in Leishmania mexicana. EMBO J **18**: 3643-3654.

Inbar, E., V.K. Hughitt, L.A. Dillon, K. Ghosh, N.M. El-Sayed & D.L. Sacks, (2017) The Transcriptome of Leishmania major Developmental Stages in Their Natural Sand Fly Vector. MBio **8**.

Jacobs, G., H. Herrmann & G. Gercken, (1982) Incorporation of [1-14C]acetate into fatty acids and aliphatic moieties of glycerolipids in Leishmania donovani promastigotes. Comparative biochemistry and physiology. B, Comparative biochemistry **73**: 367-373.

Kannan, N. & A.F. Neuwald, (2004) Evolutionary constraints associated with functional specificity of the CMGC protein kinases MAPK, CDK, GSK, SRPK, DYRK, and CK2alpha. Protein Sci **13**: 2059-2077.

Kapler, G.M., C.M. Coburn & S.M. Beverley, (1990) Stable transfection of the human parasite Leishmania major delineates a 30-kilobase region sufficient for extrachromosomal replication and expression. Mol Cell Biol **10**: 1084-1094.

Laemmli, U.K., (1970) Cleavage of structural proteins during the assembly of the head of bacteriophage T4. Nature **227**: 680-685.

Lochhead, P.A., G. Sibbet, N. Morrice & V. Cleghon, (2005) Activation-loop autophosphorylation is mediated by a novel transitional intermediate form of DYRKs. Cell **121**: 925-936.

Madeira da Silva, L. & S.M. Beverley, (2010) Expansion of the target of rapamycin (TOR) kinase family and function in Leishmania shows that TOR3 is required for acidocalcisome biogenesis and animal infectivity. Proc Natl Acad Sci U S A **107**: 11965-11970.

Margaroni, M., M. Agallou, E. Athanasiou, O. Kammona, C. Kiparissides, C. Gaitanaki & E. Karagouni, (2017) Vaccination with poly(D,L-lactide-co-glycolide) nanoparticles loaded with soluble Leishmania antigens and modified with a TNFalpha-mimicking peptide or monophosphoryl lipid A confers protection against experimental visceral leishmaniasis. Int J Nanomedicine **12**: 6169-6184.

McConville, M.J. & T. Naderer, (2011) Metabolic pathways required for the intracellular survival of Leishmania. Annu Rev Microbiol **65**: 543-561.

Mony, B.M., P. MacGregor, A. Ivens, F. Rojas, A. Cowton, J. Young, D. Horn & K. Matthews, (2014) Genome-wide dissection of the quorum sensing signalling pathway in Trypanosoma brucei. Nature **505**: 681-685.

Murakami, N., D. Bolton & Y.W. Hwang, (2009) Dyrk1A binds to multiple endocytic proteins required for formation of clathrin-coated vesicles. Biochemistry **48**: 9297-9305.

Murakami, N., D.C. Bolton, E. Kida, W. Xie & Y.W. Hwang, (2012) Phosphorylation by Dyrk1A of clathrin coated vesicle-associated proteins: identification of the substrate proteins and the effects of phosphorylation. PLoS One **7**: e34845.

Murray, H.W., J.D. Berman, C.R. Davies & N.G. Saravia, (2005) Advances in leishmaniasis. Lancet **366**: 1561-1577.

Murta, S.M., T.J. Vickers, D.A. Scott & S.M. Beverley, (2009) Methylene tetrahydrofolate dehydrogenase/cyclohydrolase and the synthesis of 10-CHO-THF are essential in Leishmania major. Mol Microbiol **71**: 1386-1401.

Nourbakhsh, F., S.R. Uliana & D.F. Smith, (1996) Characterisation and expression of a stage-regulated gene of Leishmania major. Mol Biochem Parasitol **76**: 201-213.

Papageorgiou, F.T. & K.P. Soteriadou, (2002) Expression of a novel Leishmania gene encoding a histone H1-like protein in Leishmania major modulates parasite infectivity in vitro. Infect Immun **70**: 6976-6986.

Parsons, M., E.A. Worthey, P.N. Ward & J.C. Mottram, (2005) Comparative analysis of the kinomes of three pathogenic trypanosomatids: Leishmania major, Trypanosoma brucei and Trypanosoma cruzi. BMC Genomics **6**: 127.

Petan, T., E. Jarc & M. Jusovic, (2018) Lipid Droplets in Cancer: Guardians of Fat in a Stressful World. Molecules **23**.

Pletnev, P., I. Osterman, P. Sergiev, A. Bogdanov & O. Dontsova, (2015) Survival guide: Escherichia coli in the stationary phase. Acta naturae **7**: 22-33.

Richmond, G.S., F. Gibellini, S.A. Young, L. Major, H. Denton, A. Lilley & T.K. Smith, (2010) Lipidomic analysis of bloodstream and procyclic form Trypanosoma brucei. Parasitology **137**: 1357-1392.

Sacks, D.L., S. Hieny & A. Sher, (1985) Identification of cell surface carbohydrate and antigenic changes between noninfective and infective developmental stages of Leishmania major promastigotes. J Immunol **135**: 564-569.

Sacks, D.L. & P.V. Perkins, (1984) Identification of an infective stage of Leishmania promastigotes. Science **223**: 1417-1419.

Sacks, D.L. & P.V. Perkins, (1985) Development of infective stage Leishmania promastigotes within phlebotomine sand flies. Am J Trop Med Hyg **34**: 456-459.

Sadlova, J., H.P. Price, B.A. Smith, J. Votypka, P. Volf & D.F. Smith, (2010) The stage-regulated HASPB and SHERP proteins are essential for differentiation of the protozoan parasite Leishmania major in its sand fly vector, Phlebotomus papatasi. Cell Microbiol **12**: 1765-1779.

Schmitz, M.L., A. Rodriguez-Gil & J. Hornung, (2014) Integration of stress signals by homeodomain interacting protein kinases. Biol Chem **395**: 375-386.

Serafim, T.D., A.B. Figueiredo, P.A. Costa, E.A. Marques-da-Silva, R. Goncalves, S.A. de Moura, N.F. Gontijo, S.M. da Silva, M.S. Michalick, J.R. Meyer-Fernandes, R.P. de Carvalho, S.R. Uliana, J.L. Fietto & L.C. Afonso, (2012) Leishmania metacyclogenesis is promoted in the absence of purines. PLoS Negl Trop Dis **6**: e1833.

Silva, A.M., A. Cordeiro-da-Silva & G.H. Coombs, (2011) Metabolic variation during development in culture of Leishmania donovani promastigotes. PLoS Negl Trop Dis **5**: e1451.

Smirlis, D., S.N. Bisti, E. Xingi, G. Konidou, M. Thiakaki & K.P. Soteriadou, (2006) Leishmania histone H1 overexpression delays parasite cell-cycle progression, parasite differentiation and reduces Leishmania infectivity in vivo. Mol Microbiol **60**: 1457-1473.

Smirlis, D., M. Duszenko, A.J. Ruiz, E. Scoulica, P. Bastien, N. Fasel & K. Soteriadou, (2010) Targeting essential pathways in trypanosomatids gives insights into protozoan mechanisms of cell death. Parasit Vectors **3**: 107.

Soppa, U. & W. Becker, (2015) DYRK protein kinases. Curr Biol **25**: R488-489.

Späth, G.F., L.A. Garraway, S.J. Turco & S.M. Beverley, (2003) The role(s) of lipophosphoglycan (LPG) in the establishment of Leishmania major infections in mammalian hosts. Proceedings of the National Academy of Sciences of the United States of America **100**: 9536-9541.

Stierhof, Y.D., T. Ilg, D.G. Russell, H. Hohenberg & P. Overath, (1994) Characterization of polymer release from the flagellar pocket of Leishmania mexicana promastigotes. J Cell Biol **125**: 321-331.

Tanz, S.K., I. Castleden, I.D. Small & A.H. Millar, (2013) Fluorescent protein tagging as a tool to define the subcellular distribution of proteins in plants. Front Plant Sci **4**: 214.

Tellevik, M.G., K.E. Muller, K.R. Lokken & A.H. Nerland, (2014) Detection of a broad range of Leishmania species and determination of parasite load of infected mouse by real-time PCR targeting the arginine permease gene AAP3. Acta Trop **137**: 99-104.

Tsigankov, P., P.F. Gherardini, M. Helmer-Citterich, G.F. Späth, P.J. Myler & D. Zilberstein, (2014) Regulation dynamics of Leishmania differentiation: deconvoluting signals and identifying phosphorylation trends. Mol Cell Proteomics **13**: 1787-1799.

Tsigankov, P., P.F. Gherardini, M. Helmer-Citterich, G.F. Späth & D. Zilberstein, (2013) Phosphoproteomic analysis of differentiating Leishmania parasites reveals a unique stage-specific phosphorylation motif. J Proteome Res **12**: 3405-3412.

Walther, T.C. & R.V. Farese, Jr., (2012) Lipid droplets and cellular lipid metabolism. Annual review of biochemistry **81**: 687-714.

Williams, R.A., L. Tetley, J.C. Mottram & G.H. Coombs, (2006) Cysteine peptidases CPA and CPB are vital for autophagy and differentiation in Leishmania mexicana. Mol Microbiol **61**: 655-674.

Wozencraft, A.O. & J.M. Blackwell, (1987) Increased infectivity of stationary-phase promastigotes of Leishmania donovani: correlation with enhanced C3 binding capacity and CR3-mediated attachment to host macrophages. Immunology **60**: 559-563.

Yao, C. & M.E. Wilson, (2016) Dynamics of sterol synthesis during development of Leishmania spp. parasites to their virulent form. Parasit Vectors **9**: 200.

Tables

Table 1: Fatty acid and sterol content of LinDYRK1$^{-/-}$ promastigotes and control wild type LinDYRK1$^{+/+}$ and parental LinDYRK1$^{-/-}$[pXNG-LinDYRK1] cell lines

	Mean mol % ±SD

		LinDYRK1$^{+/+}$	LinDYRK1$^{-/-}$ [pXNG-LinDYRK1]**A**	LinDYRK1^{-}$^{/-}$ **A1**	LinDYRK1^{-}$^{/-}$ **B1**
Fatty acids	14:00	1.70± 0.5	0.51 ± 0.09	0.63± 0.07	0.47± 0.32
	16:01	0.79± 0.56	0.42 ± 0.29	0.63 ± 0.19	1.10± 0.18
	16:00	8.23 ± 1.70	9.37 ± 4.25	11.71± 1.67	9.33± 0.94
	18:02	24.50± 1.70	19.24 ± 5.58	14.98 ± 6.36*	15.73± 0.52*
	18:01	41.57± 2.37	44.12 ± 3.31	41.87± 0.75	42.66± 0.29
	18:00	14.14± 0.73	17.19 ± 3.70	22.05± 3.01**	19.91± 1.68**
	C19Δ	5.46± 0.55	4.24 ±1.12	4.75± 1.12	7.12± 0.51
	20:02	2.64± 0.19	2.62± 0.00	2.09 ± 0.13	2.30± 0.06
	20:00	0.98± 0.21	2.29 ±1.68	1.29 ± 0.20	1.40± 0.09
	SFA	25.0± 3.14	29.4± 9.72	35.7± 4.81	31.1± 0.52
	MUFA	47.8± 1.26	48.8± 4.12	47.2± 1.67	50.9± 0.98
	PUFA	27.1± 1.88	21.9± 5.57	17.1± 6.48	18.0± 0.46
Sterol (retention time min^{-1})	Cholesterol (35.21)	27.66± 2.98	15.27± 0.01	14.49± 2.23	14.97± 4.66
	Zymosterol (33.59)	4.14± 0.75	7.47± 4.97	12.48± 1.28	4.51± 1.45
	Cholesta-5,7,24-trien-3β-ol (30.21)	8.57± 0.08	6.50± 1.46	7.55± 0.2	5.79± 2.37
	Ergosterol (35.21)	30.23± 0.54	29.92± 2.08	31.44± 3.82	30.83± 2.05
	Ergosta-7,24-dien-3β-ol (35.76)	11.71±0	18.66± 3.97	17.84± 0.28	22.18± 1.12
	14α-methylergosta-8,24(28)-dien-3β-ol (36.02)	4.53± 0.31	4.57± 2.22	5.38± 1.59	3.33± 0.09
	14α-methylergosta-5,7,24(28)-trien-3β-ol	6.42± 0.20	3.46± 0.79	3.80± 1.36	3.02± 0.21
	Lanosterol (36.47)	0.00± 0.00	4.99± 7.05	0.00± 0.00	8.93± 0.21
	4,14α-dimethylergosta-8,24(28)-dien-3β-ol (36.75)	2.23±0.70	3.42± 1.97	3.11± 2.94	1.67± 2.36
	Stigmasta-7,24(28)-dien-3β-ol (37.85)	4.51± 2.20	5.74± 1.71	3.91± 0.96	4.77± 1.56

Table 1 legend: Fatty acid and sterol composition was determined by GC analysis as described in "Materials and Methods" section. Data, expressed as mole percent, are means ±SD of 2 independent experiments. SFA = Saturated fatty acids, MUFA = monounsaturated fatty acids, PUFA = polyunsaturated fatty acids**. ***p< 0.01, two-tail, paired student's t test between the replicates of mutants and the corresponding control values (LinDYRK1$^{+/+}$ and LinDYRK1$^{-/-}$

[pXNG-LinDYRK1;** p=0.057, two-tail, paired Student's t test between the replicates of mutants and the corresponding control values (LinDYRK1$^{+/+}$ and LinDYRK1$^{-/-}$[pXNG-LinDYRK1).

Figure legends

Fig 1. DYRK family in Leishmania and sequence comparison of two related Leishmania DYRKs: LinDYRK1 (LinJ.15.0180) and LinJ.14.0890

(A) Representation of unrooted phylogenetic tree of DYRK kinases using as input full protein sequences. DYRK families and sub-families are indicated. The leishmanial DYRKs are highlighted according to DYRK subfamilies colour. LinDYRK1 (Lin.15.0180) is in bold red. Accession numbers are shown in **S3 Table.** (B) Sequence comparison of two related Leishmania DYRKs: LinDYRK1 (LinJ.15.0180) and LinJ.14.0890. Conserved identical residues are shaded in black. Different protein sequences or motifs are shown. PEST sequence is shown in violet [predicted by epestfind (http://emboss.bioinformatics.nl/cgi-bin/emboss/epestfind)] and DYRK homology box (DH box) in green. Secondary structure predictions (α helix blue, β sheet orange) of the kinase domains corresponding to the DYRK1A kinase domain (http:// www.rcb.org/pdb/home.home.do). Lines indicate kinase subdomains (I-XI) according to Hanks and Hunter, 1995 (Hanks & Hunter, 1995) and functional features including the ATP anchor, phosphate anchor, catalytic loop, cation binding site, activation loop, P+1 loop and CMGC insert (red line). Grey represents important insertions in the sequence of LinJ.14.0890. Red arrow represents the activation loop tyrosine (Y).

Fig 2. Localisation of GFP-LinDYRK1 in Leishmania promastigotes (A) Fluorescence confocal microscopy showing the localisation of the GFP-LinDYRK1 hybrid protein (GFP-LinDYRK1, green) in logarithmic (scale bar = 10 μm), early stationary (scale bar = 10μm) and late stationary promastigotes (scale bar upper row= 10 μm; scale bar lower row= 5 μm).

Promastigotes were stained with mitotracker (mitotracker, red) to visualise the mitochondrion and Hoechst 33342 (Hoechst, blue) to visualise the nucleus (N) and kinetoplast (K). Bright field and images with merged channels are also shown. (B) Live imaging showing the localisation of GFP-LinDYRK1 (green) L. amazonensis logarithmic promastigotes, in cells treated for 3 min with ConA-Alexa594 (ConA, red) and Hoechst (blue) to visualise the nucleus (N) and kinetoplast (K). Scale bar= 5 μM. (C) Fluorescence confocal microscopy showing the localisation of the GFP-LinDYRK1fusion protein (GFP-LinDYRK1, green) in logarithmic cells stained with FM®4-64FX (FM4-64, Red) (pulse chase experiment) for 20 min at 4^{o}C to visualise the endosomal compartment and Hoechst 33342 (Hoechst, blue) to visualise the nucleus (N) and kinetoplast (K). Bright field and images with merged channels are also shown Scale bar=10 μm, Insets: 2-fold magnification.

Fig 3. Growth-curve and cell cycle analysis of LinDYRK1 over-expressing promastigotes

(A) Growth-curve of LinDYRK1 over-expressing parasites. Left panel: 10^6 ml^{-1} starting inoculum. The growth of wild type promastigotes (LinDYRK1$^{+/+}$), of promastigotes transfected with episome only (LinDYRK1$^{+/+}$[pXNG]), of promastigotes transfected with pXNG-LinDYRK1 (LinDYRK1$^{+/+}$[pXNG-LinDYRK1]) and of promastigotes that had lost the episome after 15 passages of negative selection in GCV (LinDYRK1$^{+/+}$[pXNG-LinDYRK1]GCV), seeded at 10^6 mL^{-1} was monitored daily by cell count. Bars indicate the mean ± standard deviation (SD) of five independent experiments. Statistically significant * (*, $p < 0.05$, corresponds to comparisons will all control cells; paired two-tail Student's t test). Right panel: 3 *10^5 mL^{-1} starting inoculum. The growth of promastigotes transfected with episome only (LinDYRK1$^{+/+}$[pXNG]), of promastigotes transfected with pXNG-LinDYRK1 (LinDYRK1$^{+/+}$[pXNG-LinDYRK1]). Bars indicate the mean ± SD of three independent experiments. Statistically significant * (*, $p < 0.05$; paired two-tail Student's t test). (B) Cell cycle analysis of LinDYRK1 transgenic parasites showing overlaid histogram plots of LinDYRK1$^{+/+}$[pXNG-LinDYRK1] (light blue) and LinDYRK1$^{+/+}$[pXNG]

(pink) promastigotes. Cell cycle analysis was performed in promastigotes synchronised in the G_1/S cell boundary with 2.5 mM HU for 12 h or in promastigotes after 3 h and 6.5 h post-HU release. Diploid (2N) and tetraploid (4N) DNA content is indicated. This experiment is representative of three experiments performed.

Fig 4. Time-course analysis of LinDYRK1$^{-/-}$[pXNG-LinDYRK1] by negative GCV selection

(A) Green fluorescent histograms (FL-1) of LinDYRK1$^{-/-}$[pXNG-LinDYRK1] clones (A and B) during 4 cell culture passages with 50 μg mL^{-1} GCV (GCVp1- GCVp4) are used to quantify GFP levels and hence the presence of [pXNG-LinDYRK1]. GCV treated clones were compared to clones cultivated with 150 μg mL^{-1} of the positive selection drug, NTC (NTC). LinDYRK1$^{+/+}$ [pXNG-LinDYRK1] parasites were used as control, and wild type cells were used to determine the background fluorescence level. The perpendicular line separates GFP positive fluorescence from the background fluorescence level. (B) Histograms that show the percentage of retained GFP fluorescence for LinDYRK1$^{-/-}$[pXNG-LinDYRK1] clones A and B, of 4 passages of selection with 50 μg mL^{-1} GCV (GCVp1- GCVp4) with respect to the GFP fluorescence of the same cells treated with 150 μg mL-1 NTC (NTC). LinDYRK1$^{+/+}$ [pXNG-LinDYRK1] parasites were used as control. This experiment was performed three times and error bars represent the ± SD of three different experiments. (C) Western blot analysis after 15 passages of selection with 50 μg mL^{-1} GCV. Twenty μg of total protein was extracted from late logarithmic phase promastigotes, was analysed by immunoblotting with anti-GFP antibody (GFP, and anti-alpha tubulin antibody (alpha tubulin) for normalisation. Left: Total protein extracts were analysed from late logarithmic LinDYRK1$^{+/+}$[pXNG-LinDYRK1] pool maintained in NTC, or after 15 passages of negative selection with GCV or of passive selection (no drug). Right: Total protein extracts from individual clones derived from pools of LinDYRK1$^{-/-}$[pXNG-LinDYRK1] cells (clone B) after 15 passages of negative selection (GCV) and of the same pool cultivated in the presence of

NTC as a positive control. Here we only show the western blots derived from heterozygous clone **B**, but similar results were observed for clone **A**.

Fig 5. LinDYRK1$^{-/-}$display aberrant morphology and increased cell-death in stationary growth-phase and during heat-shock

(A) Morphology of LinDYRK1$^{-/-}$ promastigotes in stationary phase. Upper panel and lower left: Morphometric measurements showing roundness, body length and body width of LinDYRK1$^{-/-}$**A1** and **A2** clones, LinDYRK1$^{-/-}$[pXNG-LinDYRK1]A parental clone, LinDYRK1$^{-/-}$ add back (**A1** clone) and LinDYRK1$^{+/+}$ wild type cells. Bars represent mean ± SEM. At least 50 cells were counted from 3 independent experiments. Statistically significant * (*, $p < 0.01$; paired two-tail Student's t test). Lower right: Immunofluorescence analysis of stationary phase LinDYRK1$^{-/-}$ promastigotes and add back showing the morphology of alpha tubulin and DNA stained cells. Fluorescence microscopy shows nuclear and kinetoplast DNA, after labelling with Hoechst 33342 (Hoechst, blue), and alpha tubulin (α tubulin, red) after labelling with anti-alpha tubulin antibody and secondary anti-mouse Alexa Fluor® 594 (alpha tubulin, red). Scale bar= 1.5 μm. (B) DNA content determination of LinDYRK1$^{-/-}$ promastigotes in logarithmic and late stationary (day 3) growth phase by flow cytometry. Flow cytometry profiles showing the DNA content of control wild type parasites LinDYRK1$^{+/+}$, parental cell line LinDYRK1$^{-/-}$[pXNG-LinDYRK1]**A** and two independent knockout mutants LinDYRK1$^{-/-}$**A1** and LinDYRK1$^{-/-}$**A2** and the LinDYRK1$^{-/-}$**A1** add back. Diploid (2N) and tetraploid (4N) DNA content is indicated. Arrows indicate great increase of hypodiploid DNA content. This is a representative experiment of three.

Fig 6. Ultrastructural alterations and fatty acid composition in LinDYRK1 null mutants

(A) Scanning electron microscopy (SEM) of LinDYRK1 promastigotes in stationary phase. SEM showing the rounded promastigote cell shape and membrane alterations of stationary phase LinDYRK1$^{-/-}$ null mutants and comparison with wild type LinDYRK1$^{+/+}$ and parental cell line

LinDYRK1$^{-/-}$[pXNG-LinDYRK1] in the same growth phase. Arrows indicate sites of surface irregularities and membrane invaginations of null mutants. Scale bars are indicated on each image (B) Transmission electron microscopy (TEM) of LinDYRK1 promastigotes in stationary phase. TEM analysis of (I) wild type LinDYRK1$^{+/+}$, (II) LinDYRK1$^{-/-}$[pXNG-LinDYRK1] and (III-VI) LinDYRK1$^{-/-}$ stationary phase promastigotes. Figure shows increased accumulation of lipid (Ld) bodies in null mutant parasites. Black arrow in V indicates kinetoplast membrane inside a vacuole and white arrows (III, IV) show open membrane invaginations filled with lipids (IV, V). Scale bars are indicated on each image. N, nuclei; K, kinetoplast; Fp, flagellar pocket; V, vacuole. (C) Fatty acid composition of L. infantum promastigotes in stationary phase. Composition of total fatty acids isolated from LinDYRK1$^{+/+}$, LinDYRK1$^{+/+}$[pXNG-LinDYRK1] and LinDYRK1$^{-/-}$ mutants. Total fatty acids from two independent cultures of LinDYRK1$^{+/+}$, LinDYRK1$^{+/+}$[pXNG-LinDYRK1]**A** and two independent clones derived from different parental mutants LinDYRK1$^{-/-}$ **A** and LinDYRK1$^{-/-}$**B** were analysed with gas chromatography mass spectrometry (GC-MS). Bars show the mean values percentages of saturated (0 double bonds), monounsaturated (1 double bond) and polyunsaturated fatty acids (≥2 double bonds).

Fig 7. Reduction of virulent traits, compromised survival in mouse peritoneal macrophages and increased heat shock sensitivity of LinDYRK1$^{-/-}$ promastigotes

(A) Column charts displaying the percentage of lysed (propidium iodide positive, PI+) LinDYRK1$^{+/+}$, LinDYRK1$^{-/-}$[pXNG-LinDYRK1] and LinDYRK1$^{-/-}$ logarithmic (Log) and stationary (Stat) growth phase promastigotes by serum complement. Bars show the mean ± standard error of the mean (SEM) of at least three experiments performed. Statistically significant * (*, $p < 0.05$; unpaired two-tail Student's t test). (B) Column charts displaying the percentage of live (propidium iodide negative, PI-) unagglutinated LinDYRK1$^{+/+}$, LinDYRK1$^{-/-}$[pXNG-LinDYRK1] and LinDYRK1$^{-/-}$ promastigotes after PNA agglutination assay. Bars show the mean ± SD of at least three experiments performed. Statistically significant *,** (*, $p< 0.05$; **,

p<0.01; unpaired two-tail Student's t test). (C) Expression of prohibitin (LinJ.16.1710), meta 1 (LinJ.17.0990) and HASPB (LinJ23.1220) transcripts Meta-1 transcripts, relative to ribosomal protein S29 transcript (LinJ.28.2360) in stationary phase LinDYRK1$^{+/+}$, LinDYRK1$^{-/-}$[pXNG-LinDYRK1] and LinDYRK1$^{-/-}$ promastigotes by qPCR assessment. Expression levels are the mean of 3 independent experiments and error bars represent ± SEM values. Statistically significant * (*, p<0.05, paired two-tail Student's t test). (D) Cell cycle analysis of LinDYRK1$^{-/-}$ promastigotes under heat-shock. LinDYRK1$^{+/+}$, LinDYRK1$^{-/-}$[pXNG-LinDYRK1], LinDYRK1$^{-/-}$ A1 and LinDYRK1$^{-/-}$A2 and LinDYRK1$^{-/-}$ add back (**A1** clone) promastigotes in logarithmic growth phase cultivated at 26°C and 37°C for 16 h. Diploid (2N) and tetraploid (4N) DNA content is indicated. Results are representative of 3 experiments. Arrows show the increased percentage of hypodiploid cells. (E) Reduced intracellular survival in peritoneal macrophages of LinDYRK1$^{-/-}$ parasites in comparison to survival of LinDYRK1$^{-/-}$[pXNG-LinDYRK1] and LinDYRK1$^{+/+}$ promastigotes. The numbers of parasites per cell, as well as the percentage of infection at 0 h and 72 h post-infection were calculated based on the number of parasite and host nuclei. Bars show the mean ± SEM of three experiments performed. Statistically significant *,** (*, p< 0.05; **, p<0.01; unpaired two-tail Student's t test).

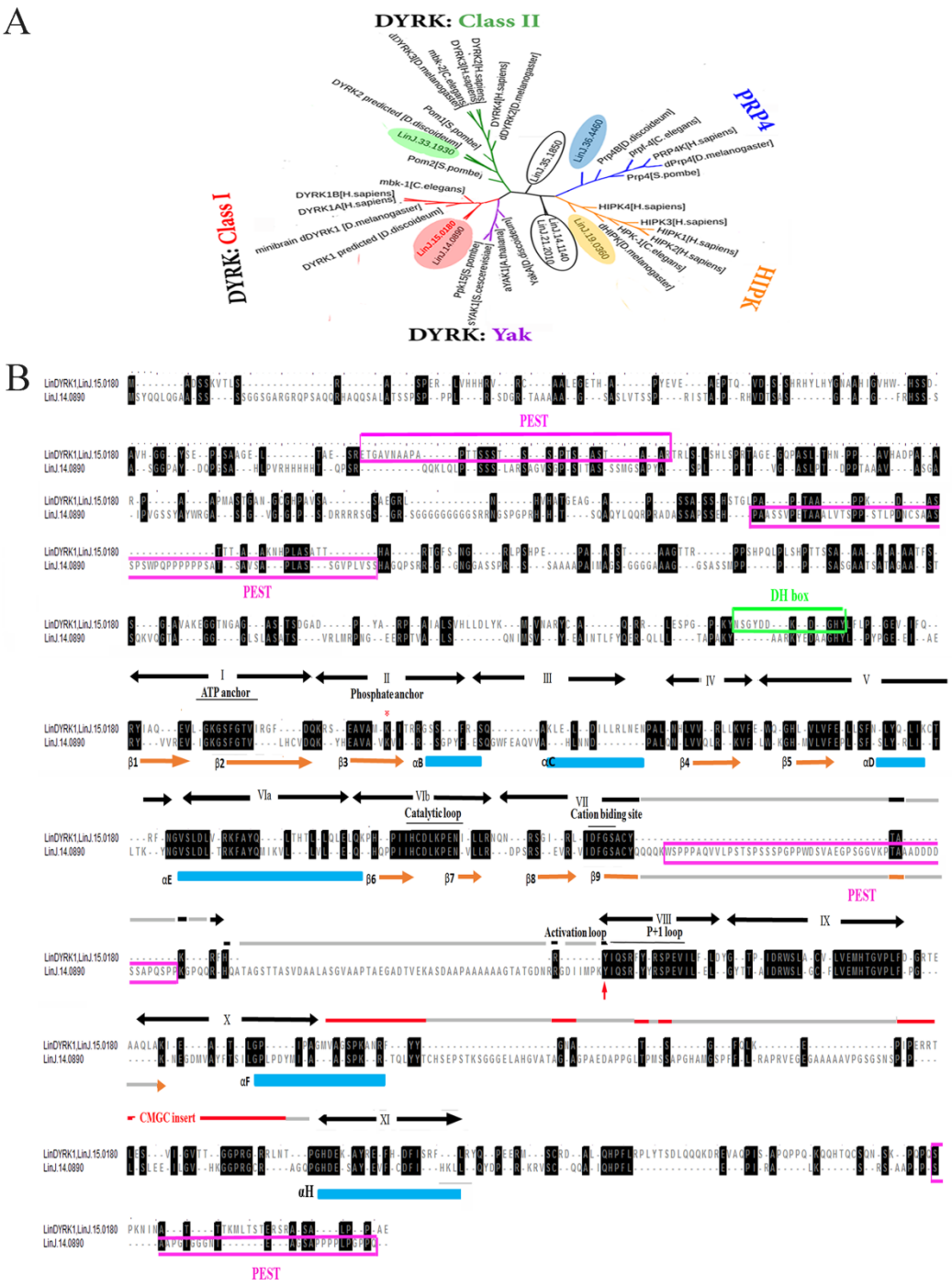

mmi_14464_f1.tif

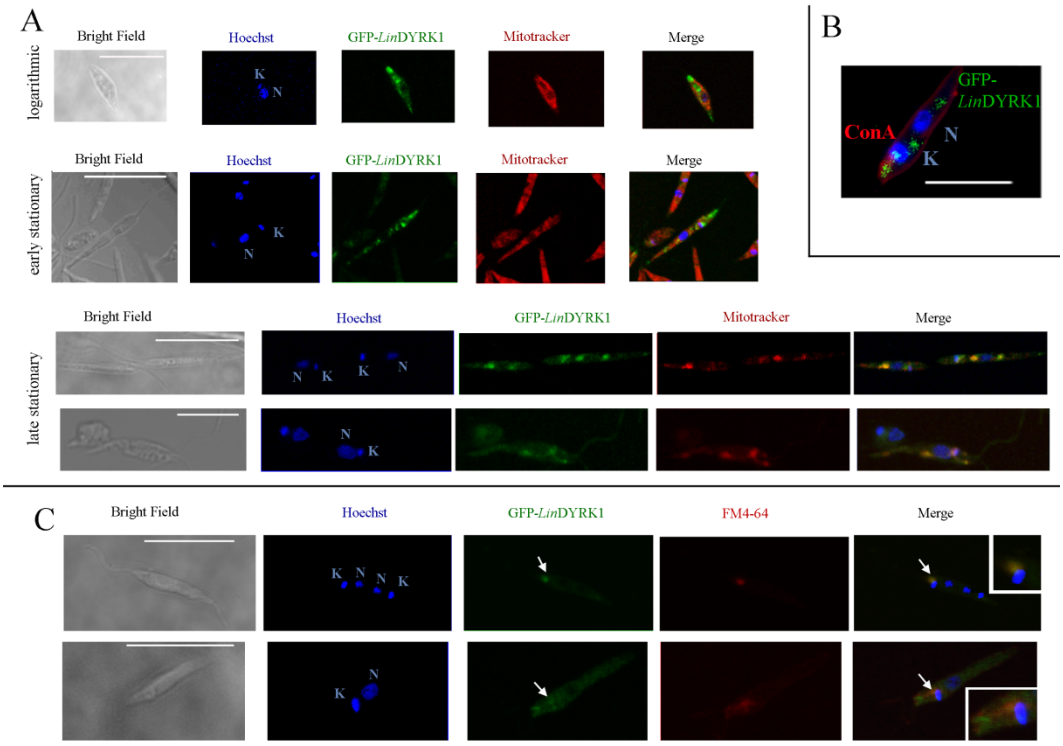

mmi_14464_f2.tif

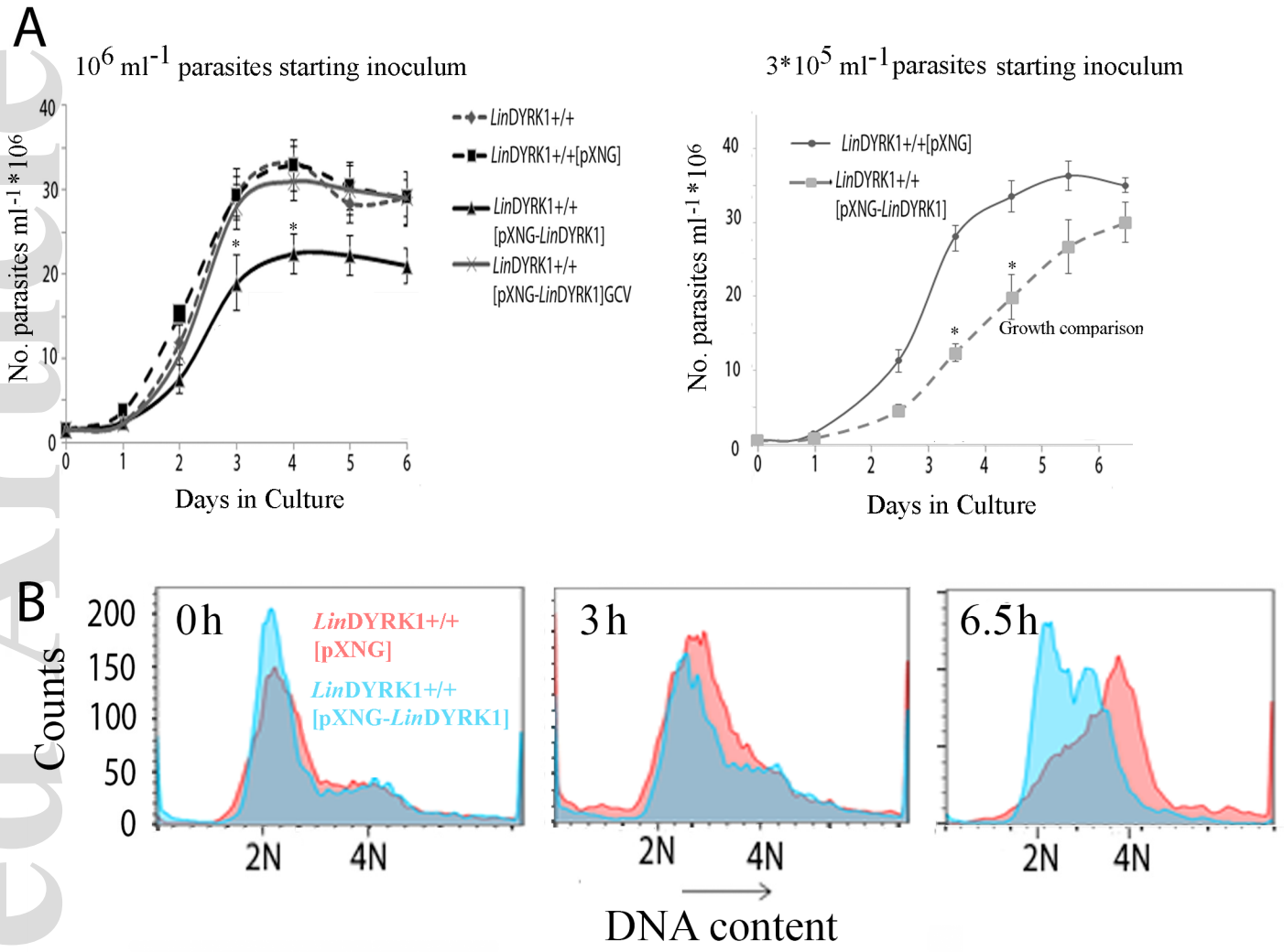

mmi_14464_f3.tif

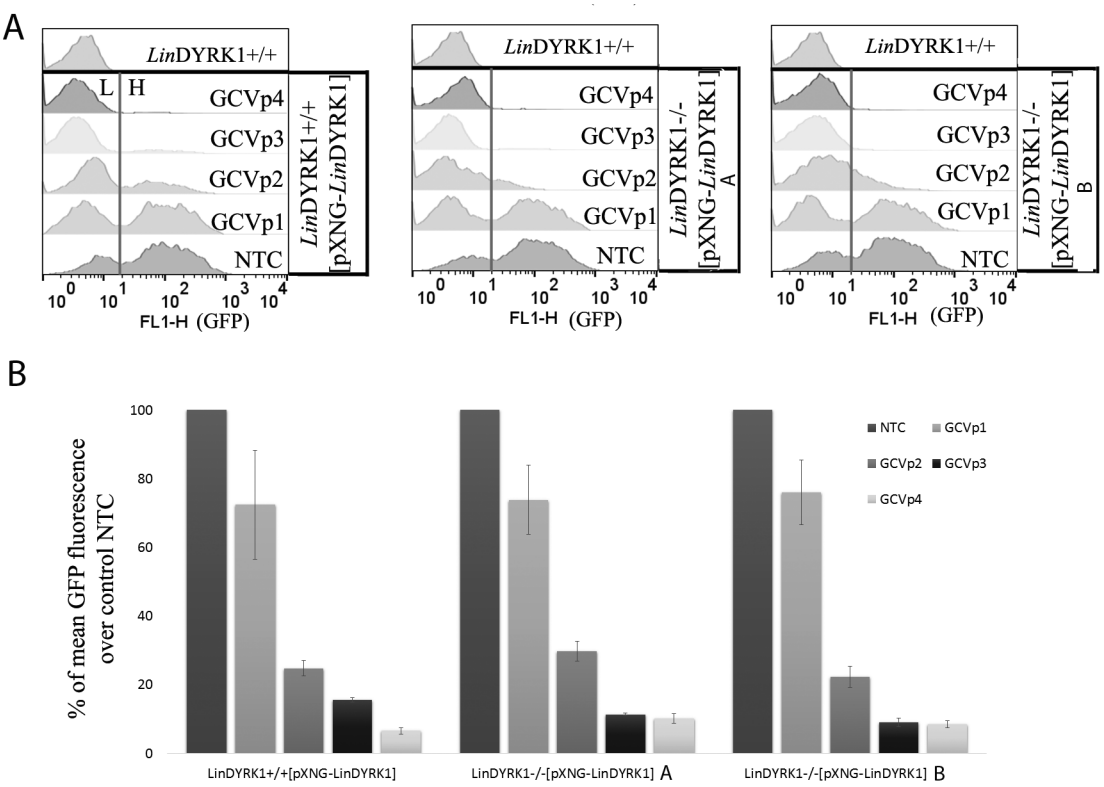

mmi_14464_f4.tif

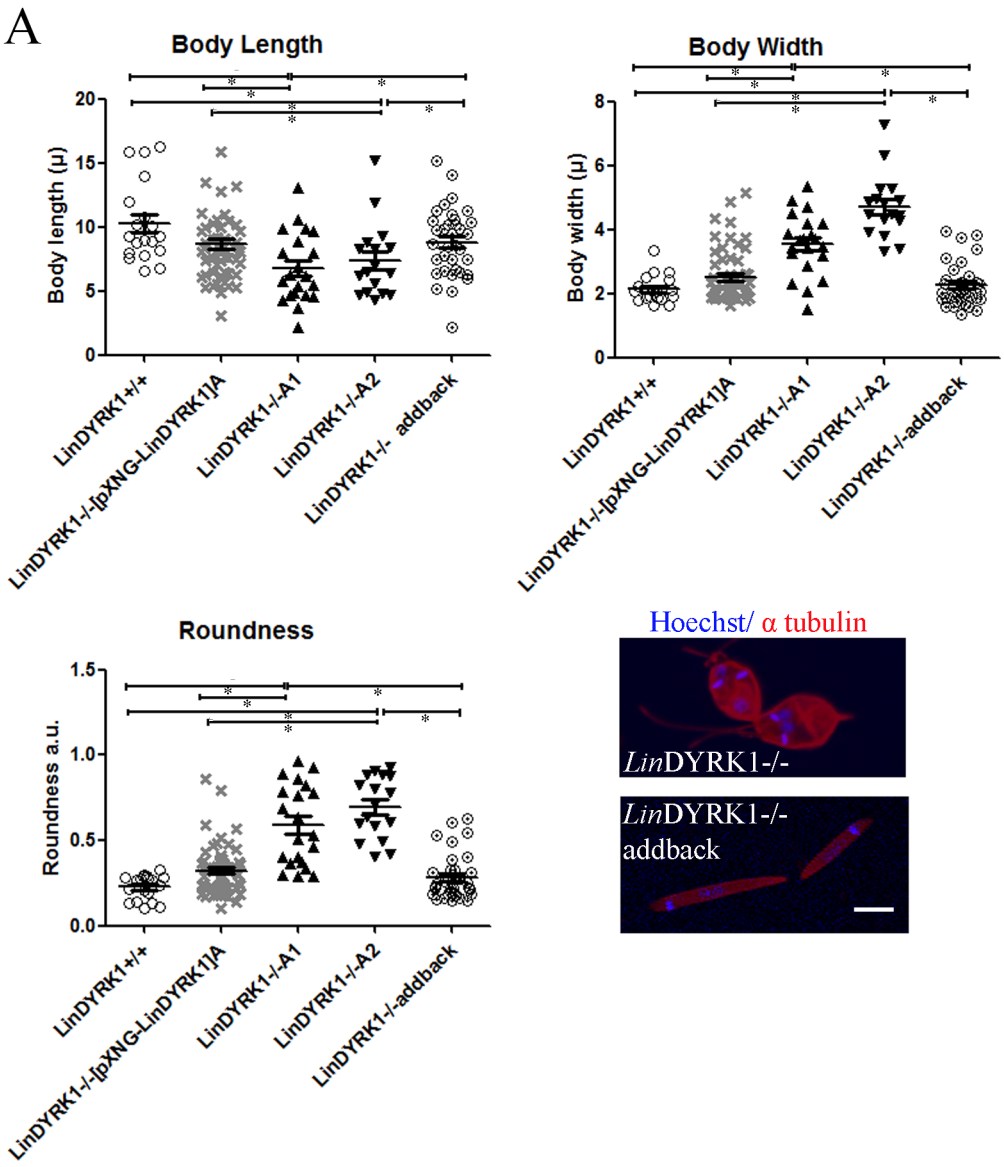

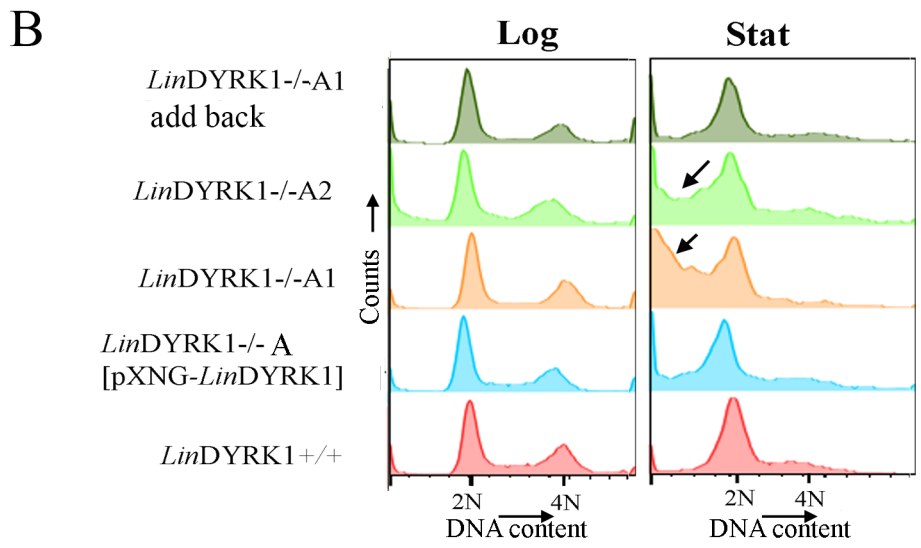

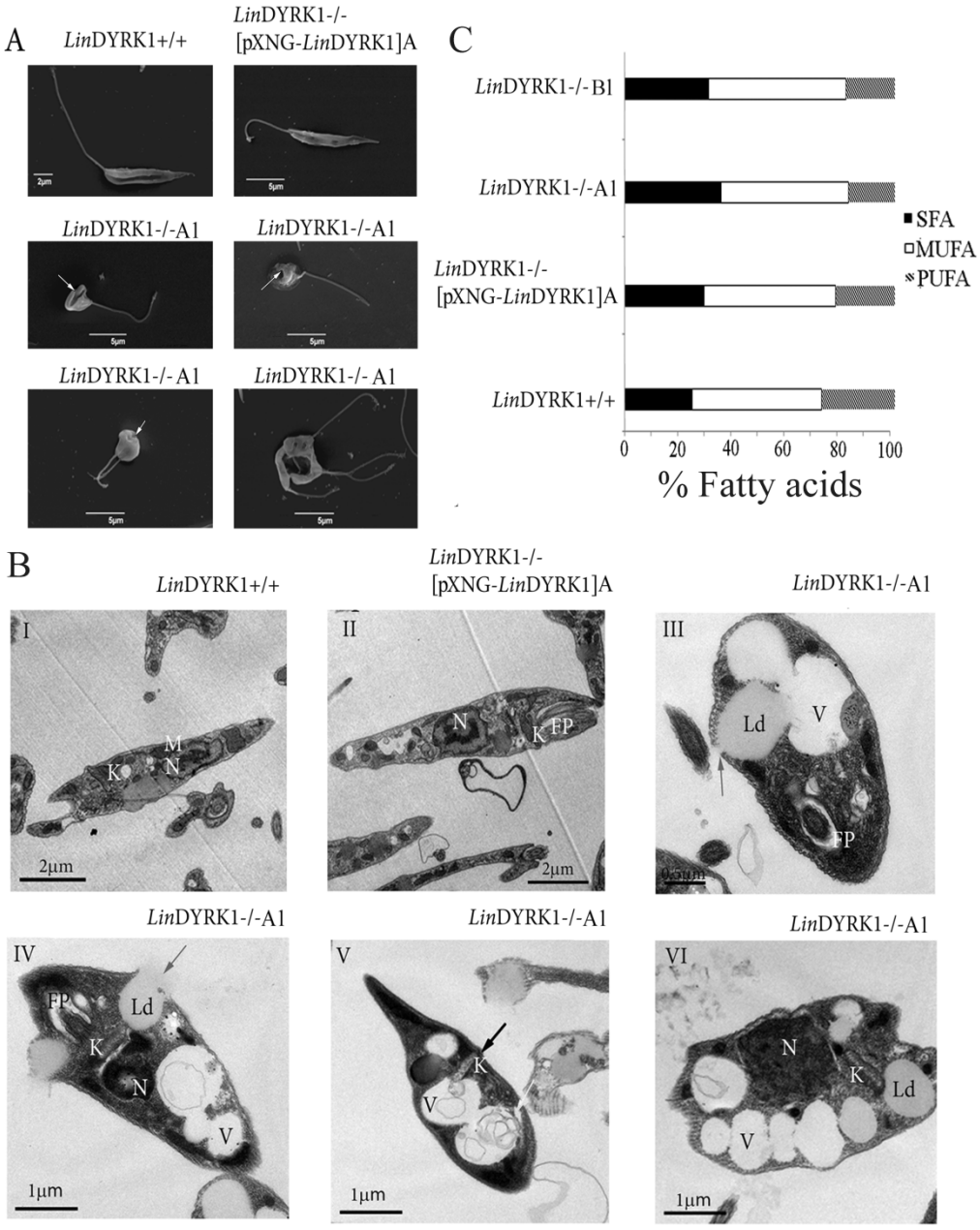

mmi_14464_f6.tif

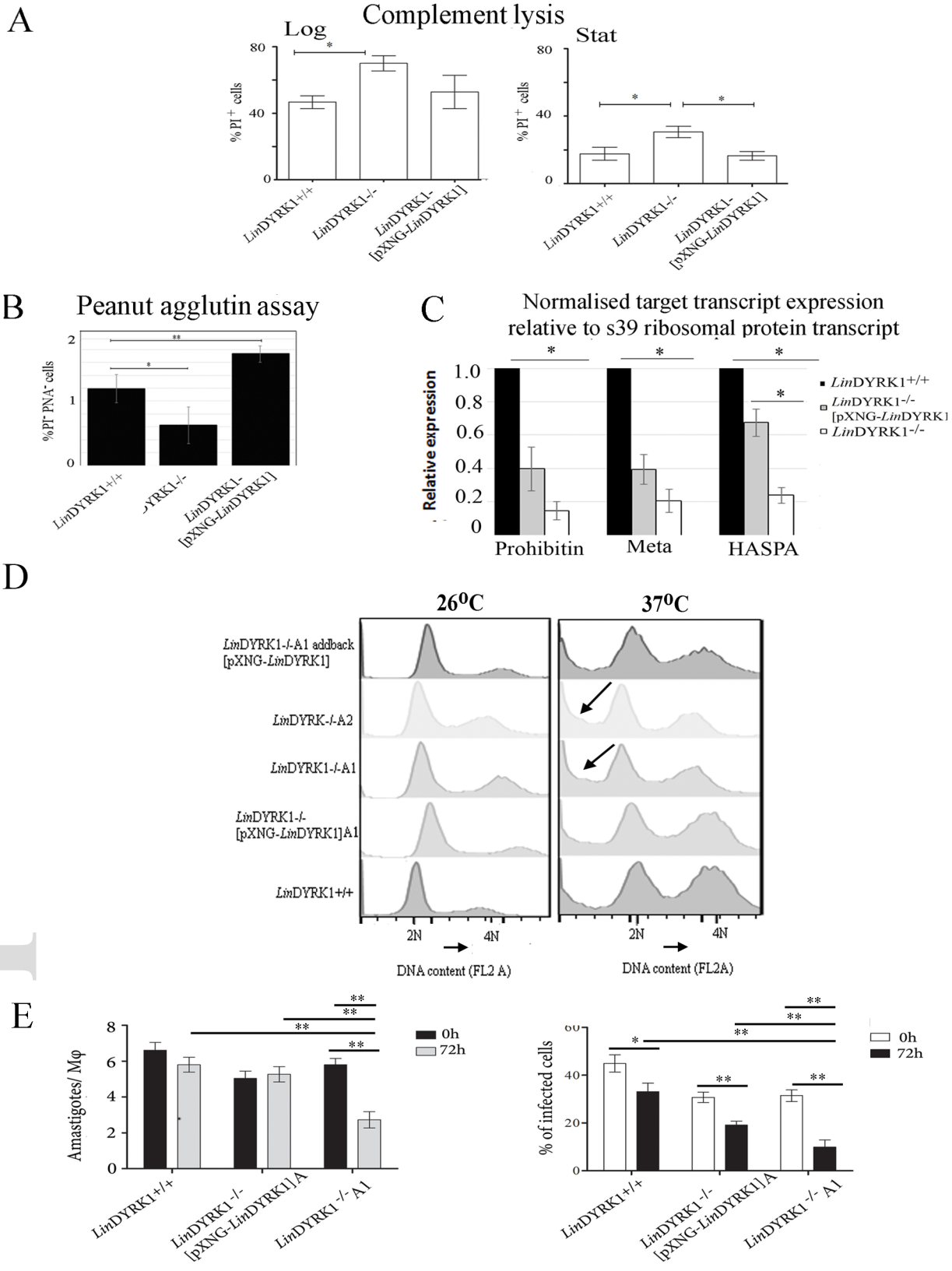

mmi_14464_f7.tif